Precambrian Research 177 (2010) 162–180

Contents lists available at ScienceDirect

Precambrian Research

journal homepage: www.elsevier.com/locate/precamres

Zircon ages of the Bayankhongor ophiolite mélange and associated rocks: Time constraints on Neoproterozoic to Cambrian accretionary and collisional orogenesis in Central Mongolia

Ping Jian[a,*], Alfred Kröner[a,b], Brian F. Windley[c], Yurao Shi[a], Fuqin Zhang[d], Laicheng Miao[d], Dondov Tomurhuu[e], Wei Zhang[a], Dunyi Liu[a]

[a] SHRIMP Centre, Institute of Geology, Chinese Academy of Geological Sciences, Baiwanzhuang Road 26, Beijing 100037, China
[b] Institut für Geowissenschaften, Universität Mainz, D-55099 Mainz, Germany
[c] Department of Geology, University of Leicester, Leicester LE1 7RH, UK
[d] Institute of Geology and Geophysics, Chinese Academy of Sciences, Beijing 100029, China
[e] Institute of Geology and Mineral Resources, Mongolian Academy of Sciences, Ulaanbaatar 210351, Mongolia

ARTICLE INFO

Article history:
Received 27 November 2008
Received in revised form 13 October 2009
Accepted 22 November 2009

Keywords:
Accretion-collision
Central Asian orogenic belt
Mongolia
Ophiolite
Syenite porphyry
Zircon

ABSTRACT

Central Mongolia is geologically characterized by close juxtaposition of an accreted oceanic terrane with an arc-microcontinent collision zone. We present new U–Pb zircon ages and geochemical data for the Bayankhongor ophiolite mélange from the oceanic terrane and for a syenite porphyry pluton from the arc-microcontinent zone, providing critical constraints on the regional evolution in late Neoproterozoic to early Cambrian times. An anorthosite (655 ± 4 Ma) associated with layered gabbro, a rodingite (metasomatized layered gabbro) (647 ± 6 Ma), and a high-level isotropic amphibole gabbro (647 ± 7 Ma) yielded the oldest zircon ages for the plutonic part of the ophiolite. A plagiogranite dike in the amphibole gabbro yielded an age of 636 ± 6 Ma, which is the youngest date obtained for the ophiolitic rocks. We suggest that the long duration (ca. 20 Ma) for formation of this plutonic sequence characterizes the sea-floor spreading evolution, and the Nd–Sr isotopic composition ($\varepsilon_{Nd(t)}$ = +7.6 to +4.7; initial $^{87}Sr/^{86}Sr$ ratio = 0.70279–0.70327) points to a mid-ocean-ridge origin. The syenite porphyry, dated at 523 ± 2 Ma, records the terminal or post-collisional phase of orogeny. The Bayankhongor oceanic lithosphere experienced at least 92 Ma of drift between its formation and accretion.

1. Introduction

Ophiolites are fragments of oceanic crust and upper mantle that have been uplifted and emplaced on continental margins or in accretionary wedges and island arcs (Robinson et al., 2008). In collisional orogenic belts such as the European Alps and the Himalayas ophiolites with complete stratigraphy (ultramafic rocks, gabbros, sheeted dykes, basalts and pelagic–clastic sediments; Anonymous, 1972) were obducted onto continental margins, generally shortly after their formation, and commonly mark plate sutures (Nicolas, 1989; Dilek, 2003). However, in many accretionary orogens dominated by accretionary wedges as in Mesozoic–Cenozoic Japan such complete ophiolite stratigraphy is rare (Isozaki et al., 1990), because the ultramafic rocks, gabbros and sheeted dykes are typically subducted (Kimura and Ludden, 1995). Consequently , accretionary wedges contain abundant fragments of basalt and pelagic–clastic sediments (Maruyama, 1997).

The Central Asian Orogenic Belt (CAOB) is a typical, wide (ca. 800 km between the Siberian and the North China cratons), long-evolving accretionary orogen (Sengör et al., 1993; Sengör and Natal'in, 1996, 2004; Kovalenko et al., 2004; Jahn et al., 2000) that comprises numerous island arcs, accretionary wedges, ophiolites and microcontinents (Badarch et al., 2002; Kröner et al., 2007; Windley et al., 2007). A major difference between the CAOB and the Mesozoic–Cenozoic of Japan is that the CAOB includes abundant, significant, distinctive ophiolite belts, as documented in northwestern China (e.g. Coleman, 1989), Mongolia (e.g. Badarch et al., 2002) and southern Siberia (Khain et al., 2002). The Mongolian ophiolites are Neoproterozoic to Palaeozoic in age (Khain et al., 2003; Tomurtogoo et al., 2006; Rippington et al., 2008), and some display a nearly complete stratigraphy. They occur in island arcs (e.g., Kuzmichev et al., 2005), accretionary wedges (e.g. Osozawa et al., 2008) and on terrane boundaries (Khain et al., 2003; Rippington et al., 2008) and thus provide a link between oceanic evolution and continental growth. Despite their tectonic importance, the

* Corresponding author. Tel.: +86 10 68999765; fax: +86 10 68311545.
E-mail address: jianping_510@yahoo.com.cn (P. Jian).

0301-9268/$ – see front matter © 2009 Elsevier B.V. All rights reserved.
doi:10.1016/j.precamres.2009.11.009

paucity of geochemical data and precise zircon ages has led to much debate about their origin, evolution, mechanism of emplacement and regional significance.

In this paper we focus on the Bayankhongor ophiolite mélange (ca. 300 km long, up to 20 km wide; Fig. 1A) in central Mongolia which is the largest and one of the best-preserved Precambrian ophiolite complexes in the CAOB (Jahn et al., 2004). The ophiolite mélange (Buchan et al., 2001, 2002; Buchan, 2002; Tomurtogoo et al., 2006; Osozawa et al., 2008) is tectonically wedged against and within 2 km-thick, accretionary complexes, namely the Delb Khairkhan mélange in the south, and the Haluut Bulag mélange in the north (Fig. 1B). These relationships are comparable to those of Cordilleran-type ophiolites (Moores, 1982; Wakabayashi and Dilek, 2003; Spaggiari et al., 2004) that are the products of subduction-accretion. Additional lithotectonic units in central Mongolia are from north to south: the late Neoproterozoic South Volcanic Belt (island arc), high-K calc-alkaline granites and an early Paleozoic syenite porphyry and, the Burd Gol mélange (late Neoproterozoic–early Cambrian Barrovian-type metamorphic belt), and the Archean to Mesoproterozoic Baidrag microcontinent (Fig. 1B). We first review these units to provide a regional framework which is characterized by close juxtaposition of an arc-microcontinent collision zone with an accreted oceanic terrane.

In order to place critical constraints on the early development of the CAOB, we report new U–Pb zircon ages and geochemical data for the Bayankhongor ophiolite (655–636 Ma) from the accreted oceanic terrane and for the early Paleozoic syenite porphyry (ca. 523 Ma) from the arc-microcontinent collision zone. The results enable us to propose a novel interpretation of the tectonic history for central Mongolia in late Neoproterozoic to early Cambrian times. We argue that accretion of a non-subductable, ophiolite-seamount/oceanic plateau terrane onto a convergent continental margin during the late stage of orogeny contributed to significant continental growth. In addition, we distinguish Permo–Triassic diabase dikes (including Triassic dikes previously interpreted as ophiolitic "sheeted dikes") and gabbros from the late Neoproterozoic Bayankhongor ophiolite. This, together with the geochemical distinction between ophiolite and post-sea floor spreading, off-ridge alkaline lavas, clearly points to a diversity of igneous formations for rocks in the Bayankhongor ophiolite mélange.

2. Geological overview

2.1. Geological outline

Buchan et al. (2001) and Tomurtogoo et al. (2006) mapped parts of the central Mongolian region (Fig. 2) and stated that the structure is dominated by a series of NW-trending, SW-dipping thrusts. These thrusts juxtaposed, from south to north, the Baidrag microcontinent, the Burd Gol mélange, the South Volcanic Belt, the Delb Khairkhan mélange, the Bayankhongor ophiolite mélange, the Haluut Bulag mélange, and the Dzag zone of the Hangai microcontinent (Fig. 1B). The main thrust separates the Delb Khairkhan mélange form the South Volcanic Belt and the Burd Gol mélange (Fig. 1B; Buchan et al., 2001).

2.1.1. Baidrag microcontinent

This ca. 500 km × 100 km microcontinent (Fig. 1A) contains Archean paragneisses, tonalitic gneisses (U–Pb zircon ages of 2650 ± 30 Ma and 2833 ± 35 Ma; Kozakov et al., 2001), granulites and amphibolites, as well as Paleoproterozoic gneisses, granulites (SHRIMP zircon age of 1826 ± 27 Ma, Demoux et al., 2009), schists, marbles, and quartzites intruded by granitic-granodioritic dikes (U–Pb zircon age of 1854 ± 5 Ma, Kotov et al., 1995), and hornblende-biotite pegmatites (U–Pb zircon age of 1825 Ma, Kozakov et al., 2001).

The Baidrag high-grade rocks are unconformably overlain on their northern side by an unmetamorphosed shelf-like sequence, at least 250 m thick dominated by stromatolite-bearing limestones that has a 4–10 m-thick basal conglomerate resting on a weathered surface of gneisses (Badarch et al., 2002).

2.1.2. Burd Gol mélange

To the north of the sedimentary shelf sequence is the ca. 30 km-wide Burd Gol mélange (Fig. 1B) that includes chlorite-muscovite schists, chlorite schists, chlorite-biotite schists, phyllites, slates, and graphite-rich chlorite schists, which contain numerous blocks of deformed calc-turbidite, marble, shale, sandstone, quartzite, conglomerate, chert, chloritic basalt and gabbro. The schists dip shallowly to the northeast. The mélange contains brittle to ductile shear zones and is cut by many gold-bearing quartz veins up to 60 m wide.

The mélange underwent Barrovian-type metamorphism (Buchan et al., 2001); through a distance of about 6 km the metamorphic grade increases northwards towards the thrust contact with the South Volcanic Belt, from greenschist- to upper amphibolite-facies, marked by the progressive appearance of biotite, garnet, staurolite, kyanite, and sillimanite.

Although Mitrofanov et al. (1981) considered that the Burd Gol mélange formed part of a continental margin against the Neoproterozoic shelf sequence, the overall geological features suggest formation in a subduction-accretion complex (Buchan et al., 2001, and references therein), and in particular in an accretionary wedge. We emphasize the Barrovian-type metamorphism which is commonly considered to be indicative of collisional orogenesis as documented in the Caledonides of Scotland (Thompson and England, 1984) and the NW Iberian Massif (Arenas and Martínez Catalán, 2003).

Using the evaporation method, Demoux et al. (2009) analyzed detrital zircons from a fine-grained quartzitic lens from the mélange. The $^{207}Pb/^{206}Pb$ ages ($n = 13$) range between 1017 and 2023 Ma and suggest a maximum earliest Neoproterozoic depositional age and a heterogeneous sedimentary source dating to the Paleoproterozoic. Kozakov et al. (2006) reported a TIMS U–Pb zircon age of 562 ± 2 Ma for a syntectonic kyanite-bearing pegmatite vein in a kyanite–sillimanite schist and interpreted this age to represent the time of Barrovian-type metamorphism (see also Kovach et al., 2005; Demoux et al., 2009). A biotite from a gneiss has a $^{40}Ar/^{39}Ar$ plateau age of 533 ± 3 Ma (Buchan et al., 2002, and references therein). This value is younger than, but broadly similar to, the 562 ± 2 Ma zircon age. These isotopic age data roughly constrain the peak metamorphism between ca. 562 and ca. 533 Ma.

2.1.3. South Volcanic Belt

On the boundary between the Burd Gol mélange and the Delb Khairkhan mélange, there is a slice of volcanic rocks (the South Volcanic Belt, Fig. 1B) which is unconformably overlain by a well-bedded limestone–quartzite–mudstone sequence about 2000 m thick (Fig. 2A and B) (Buchan et al., 2001). On its northern side the volcanic belt is separated from the Delb Khairkhan mélange by a ca. 1 km-wide mylonite along a thrust (Fig. 1B).

The volcanic rocks include sheet-like flows, up to 15 m thick, of andesite, dacite, basalt, and trachybasalt, which are interbedded with, and topped by, agglomerate, sandstone and tuff. These volcanic and sedimentary strata are consistent with those of an island arc (e.g. Bailey, 1981; Macdonald et al., 2000). The agglomerates contain 2–5 cm angular fragments of most of the volcanic rocks and are transected by a major network of dikes of K-feldspar granite and rhyolite, each up to several meters wide, and there are small intrusive bodies of quartz-plagioclase porphyry.

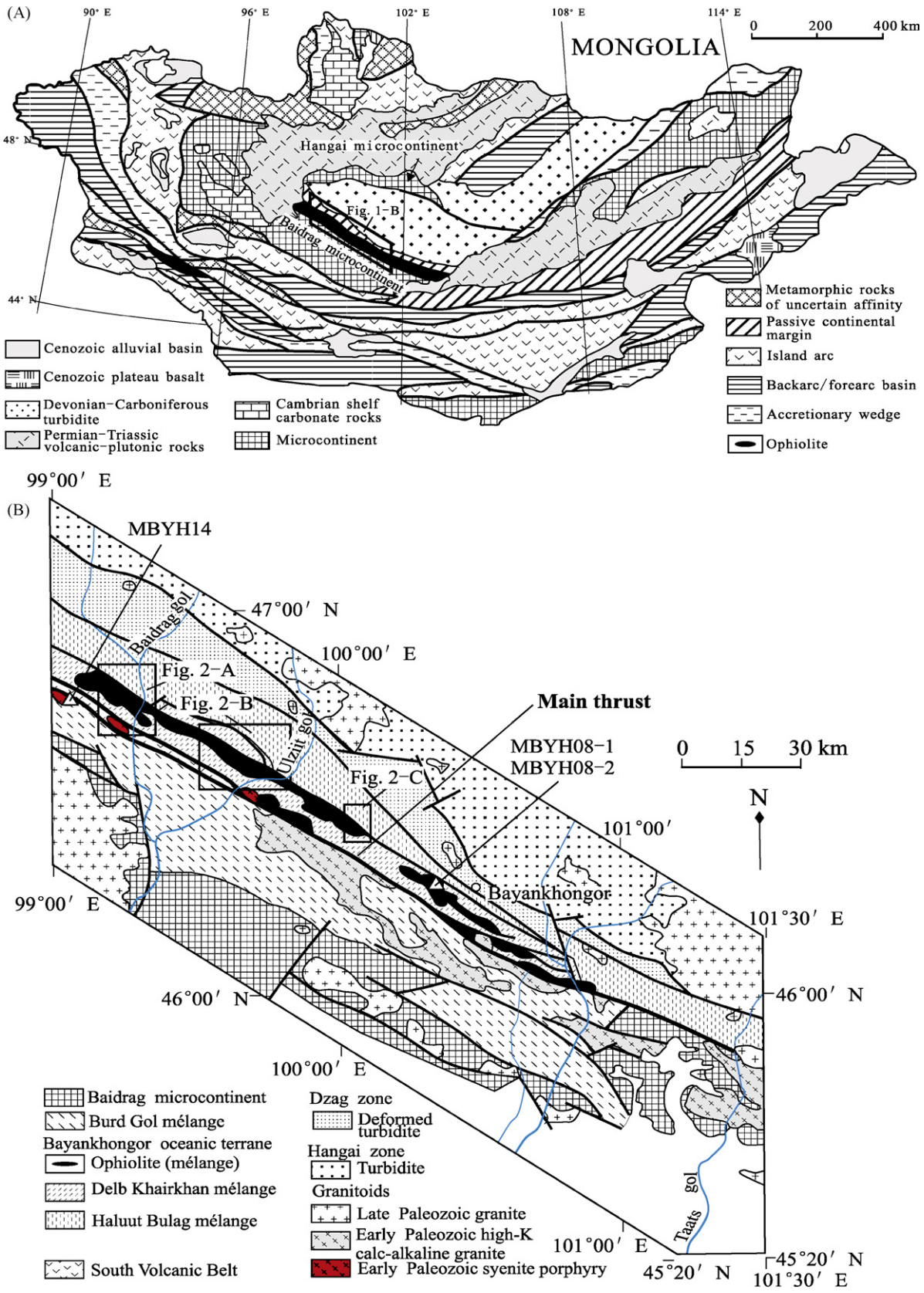

Fig. 1. (A) Terrane map of Mongolia (after Badarch et al., 2002). Position of (B), Baidrag and Hangai microcontinents are indicated. (B) Geological map of the Bayankhongor area, complied after Buchan et al. (2001) and Tomurtogoo et al. (2006). The positions of geological maps and cross-sections (Fig. 2A–C) and some analyzed samples (MBYH08-1, MBYH08-2 and MBYH14) are marked.

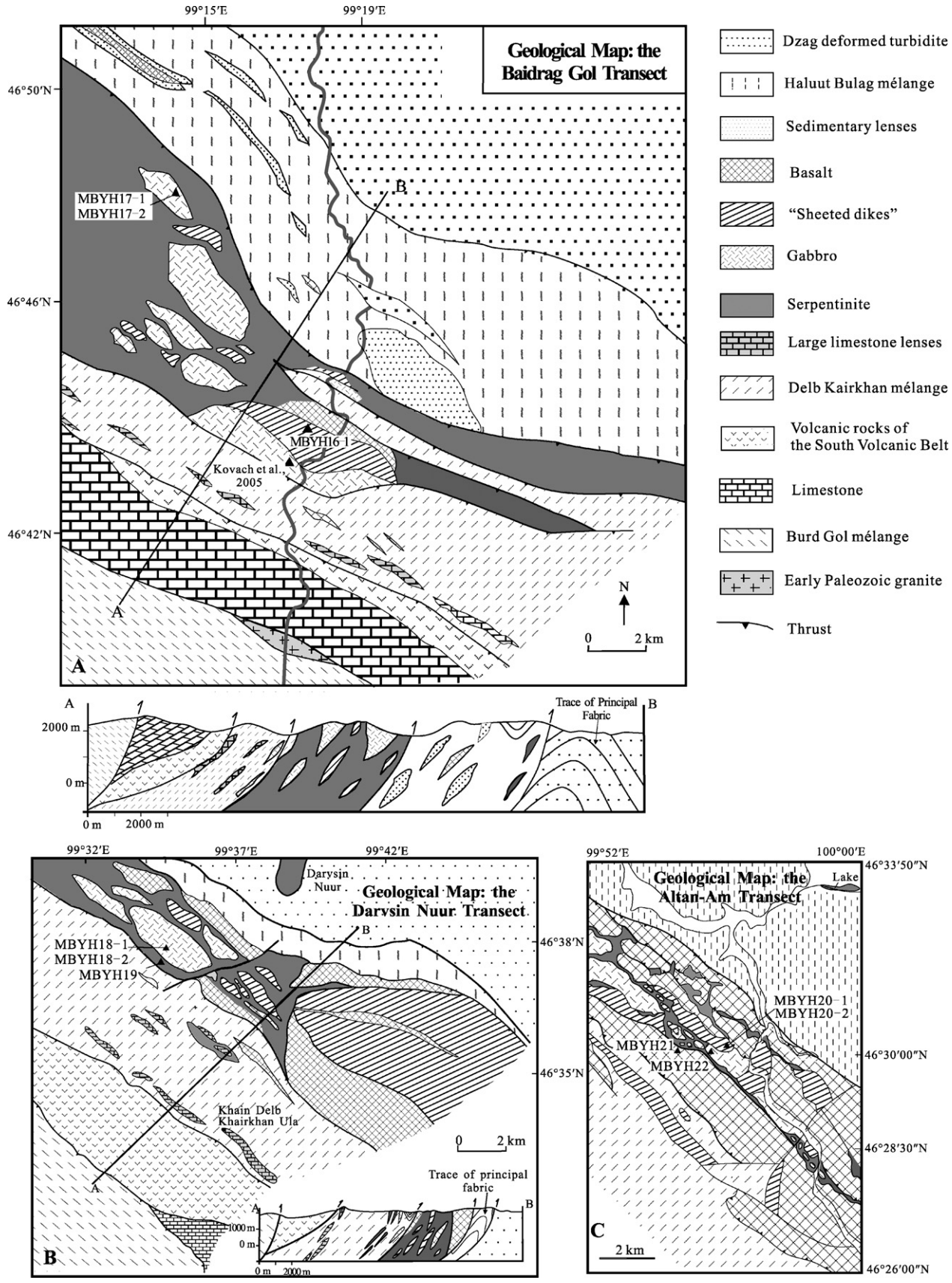

Fig. 2. (A) Geological map and cross-section of the Baidrig Gol transect (after Buchan et al., 2001). The positions of samples MBYH17-1, MBYH17-2, MBYH16-1 and the anorthosite sample of Kovach et al. (2005) are marked. (B) Geological map with a cross-section of the Darvsin Nuur transect (after Buchan et al., 2001). Samples MBYH18-1, MBYH18-2 and MBYH19 are indicated. (C) Geological map of the Atlan Am area (after Tomurtogoo et al., 2006). The positions of samples MBYH20-1, MBYH20-2, MBYH21 and MBYH22 are marked.

Geochemical data by Buchan (2002) indicate that the volcanic rocks are enriched in LILE (large-ion lithophile elements, such as Rb, Ba) and LREE (light rare earth elements; $La_n/Yb_n = 2.1–20.3$). Their trace element patterns exhibit pronounced negative Nb and Ti anomalies, consistent with an island arc origin. An andesite and two dacites have positive ε_{Nd} ($t = 500$ Ma) values of +0.7 to +5.9.

The age of the South Volcanic Belt has previously been considered to be late Precambrian (Riphean in Russian terminology), Ordovician or Devonian, based on paleontological evidence (see Tomurtogoo et al., 2006, for review). A cross-cutting rhyolite dike has a $^{207}Pb/^{206}Pb$ zircon evaporation age of 474 ± 8 Ma, but recently A. Kröner (pers. comm.) obtained a SHRIMP zircon age of 544 ± 7 Ma for a rhyolitic lava from the volcanic belt at the contact between the Burd Gol and Delb Khairhan mélanges. Although the precise age of arc volcanism of the South Volcanic Belt is still uncertain, we believe that this new result updates the minimum age of arc volcanism.

2.1.4. The Delb Khairkhan and Haluut Bulag mélanges

The Bayankhongor ophiolite is tectonically dismembered and is in fault contact with, and tectonically wedged between, the Delb Khairkhan and the Haluut Bulag mélanges (Osozawa et al., 2008). The Delb Khairkhan mélange contains lenses of igneous, sedimentary (Buchan et al., 2001), and metamorphic (greenschist- to amphibolite-facies; Osozawa et al., 2008) rocks, enclosed in a turbidite matrix. Ophiolitic rocks as well as rocks from the South Volcanic belt occur as blocks within the mélange (Buchan et al., 2001). Along its southern side the mélange contains lenses, up to several kilometers long, of limestone interbedded with shale and mudstone that together have a maximum thickness of about 1 km. Limestones occur in small lenses throughout the mélange.

The Haluut Bulag mélange contains lenses of limestone, sandstone, radiolarian chert, tuff, minor felsic volcanic rocks, and vesicular basalt within a matrix of phyllite or mica schist (Buchan et al., 2001). The vesicular basalt is overlain by limestone associated with radiolarian chert, an assemblage suggesting a seamount origin. According to Osozawa et al. (2008), the first radiolaria appears in Cambrian sediments, and the formation age of the Haluut Bulag mélange is no older than Cambrian (542 Ma). Some well-preserved pillow basalts in the adjacent Bayankhongor ophiolite mélange contain inter-pillow limestone and chert, and are locally overlain by bedded black chert and limestone of lower Cambrian age (Buchan et al., 2001).

2.1.5. Dzag zone

This zone contains greenschist-facies pelitic and psammitic schists that contain recognizable sedimentary lithologies such as green, cm-thick sandstone beds (the green color is due to a high content of detrital chlorite) with quartz pebbles and grading, which alternate with 1 cm-thick siltstone beds (Buchan et al., 2001; Tomurtogoo et al., 2006). The schists are dominated by a well-developed SW-dipping shear fabric, NE-vergent asymmetric folds, and NE-directed overthrusts (Badarch et al., 2002; see also Jahn et al., 2004). The zone is separated from the Bayankhongor ophiolite mélange by the overlying Haluut Bulag mélange with its seamount blocks (Osozawa et al., 2008).

A. Kröner and A. Demoux (pers. comm.) recently dated detrital zircons from two Dzag chlorite schist samples by SHRIMP and LA-ICP-MS. Their ages vary from 446 to 2613 Ma ($n = 80$), indicating a maximum mid-Ordovician (ca. 446 Ma) depositional age and a heterogeneous, Neoproterozoic to Neoarchean sedimentary provenance. The most likely source region is the continental margin of the Hangai microcontinent to the north (Fig. 1A) that contains gneiss, migmatite, amphibolite, anorthosite, and volcaniclastic rocks of Neoarchean to Neoproterozoic age (Badarch et al., 2002).

Metamorphic white micas from the Dzag metasediments have K–Ar ages of 454 ± 9 Ma, 445 ± 9 Ma (Kurimoto and Tungalag, 1998), 440 ± 22 Ma and 395 ± 20 Ma (Teraoka et al., 1996; see also Jahn et al., 2004). These dates are generally younger than, but overlap with, the ca. 446 Ma maximum age of deposition. Therefore, regional metamorphism is likely to have begun almost immediately after deposition.

2.2. Bayankhongor ophiolite mélange

Buchan et al. (2001) and Tomurtogoo et al. (2006) suggested that the Bayankhongor ophiolite mélange contains a complete ophiolite stratigraphy, i.e. ultramafic cumulates, gabbro, sheeted dikes, pillow basalt and chert, all these lithologies occurring as blocks within a serpentinite matrix (Fig. 2A–C). The ultramafic rocks include serpentinized harzburgite, dunite, wehrlite, clinopyroxenite and orthopyroxenite. The gabbros contain inter-layered parts with anorthosite, foliated gabbro, and isotropic gabbro containing plagiogranite. A "sheeted dike complex" with plagiophyric and aphyric dikes is well preserved and clearly demonstrates dike-in-dike relationships. However, as shown in this paper, these are much younger than the ophiolite components and we therefore use this term in inverted commas.

An amphibole gabbro has a Sm–Nd isochron (whole-rock + mineral) age of 569 ± 21 Ma (Kepezhinskas et al., 1991). This age has been widely cited as the formation age of the ophiolite, but has not been confirmed by later data. A weighted mean SHRIMP zircon $^{206}Pb/^{238}U$ age of 665 ± 15 Ma was obtained for an anorthosite (Kovach et al., 2005) that forms a lenticular body within layered gabbro (46°43.233′N, 99°17.274′E, see Fig. 2A). This provides, for the first time, a reliable age constraint on the igneous formation of the ophiolite; however, the uncertainty is large, and the MSWD is unreasonably small (ca. 0.1), and we have therefore recalculated the analyses (see Section 5.1.1). Metamorphic amphibole that defines a lineation within pillow basalt has an Ar–Ar age of 484.5 ± 5.9 Ma, suggesting that the ophiolite was undergoing deformation at this time (Buchan et al., 2002, and references therein).

It is noteworthy that significant differences in geochemistry and geology between the currently described Bayankhongor ophiolite (actually mélange) and typical ophiolites (Anonymous, 1972) are apparent. The first important difference is that the basaltic lavas include both tholeiitic and alkaline varieties (Tomurtogoo et al., 2006). Tholeiitic lavas range in composition from picrobasalt, through dominant basalt to rare basaltic andesite, and are akin to NMORB (normal mid-ocean-ridge basalt) or EMORB (enriched mid-ocean-ridge basalt). The alkaline lavas comprise basanite, trachybasalt and trachyandesite that are characterized by high TiO_2 contents up to 3%, and a transitional EMORB/OIB geochemical affinity (Kovach et al., 2005), features that suggest a significant contribution from an enriched mantle source.

The Bayankhongor ophiolite has been well known for its "sheeted dikes" (e.g. Buchan et al., 2001; Tomurtogoo et al., 2006). In most cases, these dikes (dike-in-dike complex, up to 1.2 km wide) are tectonically in contact with gabbros and basaltic lavas or intrude ultramafic rocks (Buchan et al., 2001; Tomurtogoo et al., 2006) (see Fig. 2A–C). Such occurrence is obviously inconsistent with ophiolitic sheeted dikes, which occupy the transitional zone directly below pillow basalts and above high-level, isotropic gabbros (Abbotts, 1981; Coleman, 1977; Dilek et al., 1997). Hence, their origin with respect to the ophiolite is uncertain. We try to solve this enigma below by geochemical analysis and zircon dating (see Sections 4.2 and 5.2).

2.3. Granites

Several early Paleozoic, high-K calc-alkaline, peraluminous, elongate granite bodies (Buchan et al., 2002; Jahn et al., 2004)

have intruded the Burd Gol mélange, the South Volcanic Belt and the Baidrag microcontinent; many are associated with major thrusts (Fig. 1B). Buchan et al. (2002) obtained zircon evaporation $^{207}Pb/^{206}Pb$ ages of 539 ± 1 Ma, 539 ± 5 Ma and 545 ± 2 Ma for a granite that intrudes the Burd Gol mélange. These data are not included in the following discussion, because the evaporation method reports a $^{207}Pb/^{206}Pb$ age, whereas the SHRIMP method usually reports a weighted mean $^{206}Pb/^{238}U$ age for rocks younger than 1000 Ma (Black and Jagodzinski, 2003); these two values are not always comparable unless the zircon has an ideally closed U–Pb system and contains no inherited components.

SHRIMP dating of magmatic zircons from a monzogranite sample of the Tsagaan pluton (location: 46°21.81′N; 99°44.36′E) yielded a weighted mean $^{206}Pb/^{238}U$ age of 514 ± 10 Ma (n = 14) (Jahn et al., 2004), which we accept to represent the emplacement age of this high-K calc-alkaline granite. The granite also has inherited zircons with ages of ca. 558–646 Ma (5 grains) and ca. 816–1771 Ma (6 grains) (Jahn et al., 2004). According to Buchan et al. (2002) and Jahn et al. (2004), these granites have negative $\varepsilon_{Nd(t)}$ values of −3.1 to −7.1 and initial $^{87}Sr/^{86}Sr$ ratios of 0.7077–0.7078, suggesting participation of old crust in the magma generation.

Small bodies of syenite porphyry occur along the Burd Gol mélange/South Volcanic Belt boundary (Fig. 1B), and were geochemically and geochronologically studied as an important part of this work.

Late Paleozoic and early Mesozoic undeformed granites that are widespread in the region (Fig. 1B) are characterized by near-zero $\varepsilon_{Nd(t)}$ values (0 to −2) (Jahn et al., 2004).

3. Field occurrence, sampling and petrology

Most of our samples were collected along cross-strike transects of the Baidrag Gol (river) (Fig. 2A, Buchan et al., 2001), Davsin Nuur (Fig. 2B, Buchan et al., 2001), and Altan Am (Fig. 2C; Tomurtogoo et al., 2006). In addition, a coarse-grained gabbro (MBYH08-1), a diabase dike (MBYH08-2), and a syenite porphyry (MBYH14) were collected outside of the three areas, and their locations are shown in Fig. 1-B.

3.1. Gabbroic blocks

3.1.1. Rodingite and leucogabbro dike

Rodingite (46°46′41.1″N, 99°15′35.75″E; Fig. 2A) was recognized in the field by the presence of reddish-brown garnet (Fig. 3A and B). The principal minerals are garnet and clinopyroxene (white), with subordinate epidote, amphibole, chlorite and calcite. Locally, the garnet-rich rodingite contains xenoliths of pyroxenite (Fig. 3A) and grades into layered gabbro with anorthosite pods (Fig. 3B). Garnet and clinopyroxene locally form large lenses, and a banding defined by the preferred orientation of clinopyroxene and modal variation in garnet and pyroxene is characteristic of the dated rodingite sample (MBYH17-1) (see Fig. 3B). Rodingite is a Ca-rich, SiO_2-undersaturated rock, composed of Ca–Al and Ca–Mg silicates; it is formed by Ca-metasomatism (of various silicate rock types) that accompanies low-temperature serpentinization (Coleman, 1977) at an early stage of ocean crust evolution (e.g., Dubińskaa et al., 2004).

The rodingite-gabbro is intruded by a swarm of doleritic and gabbroic dikes. A leucogabbro dike (ca. 1 m wide) (MBYH17-2) was collected for zircon dating.

3.1.2. Amphibole gabbro and plagiogranite

In the Darvsin Nuur transect (Fig. 2B), several blocks of isotropic amphibole gabbro (MBYH18-1) and plagiogranite (MBYH18-2) were sampled from the same outcrop (Fig. 3C) (46°38′12.9″N, 99°33′43.8″E). The amphibole gabbro contains near-equal amounts of clinopyroxene, plagioclase and amphibole as well as minor opaque minerals (ca. 5%), and secondary epidote, chlorite and calcite. Plagiogranite, which occurs as veins of variable width (ca. 0.1–0.4 m) within the amphibole gabbro, is granular, medium-grained, and predominantly consists of plagioclase (>65 modal%) and subordinate quartz (ca. 30%); secondary minerals are epidote, chlorite and calcite.

3.1.3. Coarse-grained gabbro and diabase dike

From Bayankhongor town to the east, the ophiolite becomes largely dismembered, and sporadic outcrops of ophiolite lithologies are surrounded by shale and limestone (Buchan et al., 2001). Several samples were taken from ca. 10 km west of Bayankhongor town (46°06′34.2″N, 100°35′01.5″ E; Fig. 1B), where a gabbro (MBYH08-1) block is intruded by diabase (MBYH08-2) dikes (Fig. 3D). Sample MBYH08-1 is a coarse-grained (ca. 0.5–1.5 cm grain size) gabbro with a poikilitic texture and equal contents of plagioclase and clinopyroxene. Narrow mafic and felsic veinlets are too pervasive to be precluded in sampling. Sample MBYH08-2 is a fresh, fine-grained diabase dike with an ophitic texture.

3.2. "Sheeted dikes"

Plagiophyric dike sample MBYH16-1 (46°43′54.3″N, 99°18′10.5″E; Fig. 2A) contains abundant plagioclase and clinopyroxene megacrysts (both up to 0.5–1.5 cm across) that are set in a basaltic matrix (Fig. 3E). Samples MBYH 20-1 and MBYH20-2 are plagiophyric (MBYH 20-1) and aphyric (MBYH20-2) dikes (Fig. 3F) respectively, from the Altan Am area (46°30′16.1″N, 99°56′30.9″E; Fig. 2C).

3.3. Porphyritic gabbro

In the Altan Am area isotropic gabbros are locally in tectonic contact with, and locally transitional into pillow lava (e.g. sample MBYH 21, 46°30′34.6″N; 99°55′22.2″E). These gabbros were previously assumed to be part of the Bayankhongor ophiolite (Tomurtogoo et al., 2006), but their dominant rock type, i.e., a porphyritic gabbro, is peculiar to any known ophiolite. Our sample MBYH22 (46°30′28.7″N, 99°55′18.1″E) contains plagioclase crystals up to 3 cm in size (Fig. 3G).

3.4. Syenite porphyry

This sample was collected from approximately 15 km west of Baidrag Gol (46°44′48.7″N, 99°07′37.7″E). The syenite porphyry (marked in red in Fig. 1B (For interpretation of the references to color in this figure legend, the reader is referred to the web version of the article.)) occurs along the South Volcanic Belt/Burd Gol mélange boundary and is foliated. The studied syenite porphyry intrudes the Burd Gol mélange and is a red, porphyritic rock (Fig. 3H). Orthoclase and sanidine constitute large, elongated crystals, which are surrounded by a matrix of fine-grained orthoclase, rare plagioclase, and well-oriented dark minerals (amphibole, biotite and epidote).

4. Geochemical data

Major and trace elements were analyzed in the Laboratory of Continental Dynamics, Northwest University, Xian, China, by standard XRF techniques and with an ICP-MS with Elan 6100DRC plasma. Analytical uncertainties are ~1.5% for major elements, and ~5–15% for trace elements depending on concentration level. Nd and Sr isotopes on whole-rock samples were determined at the

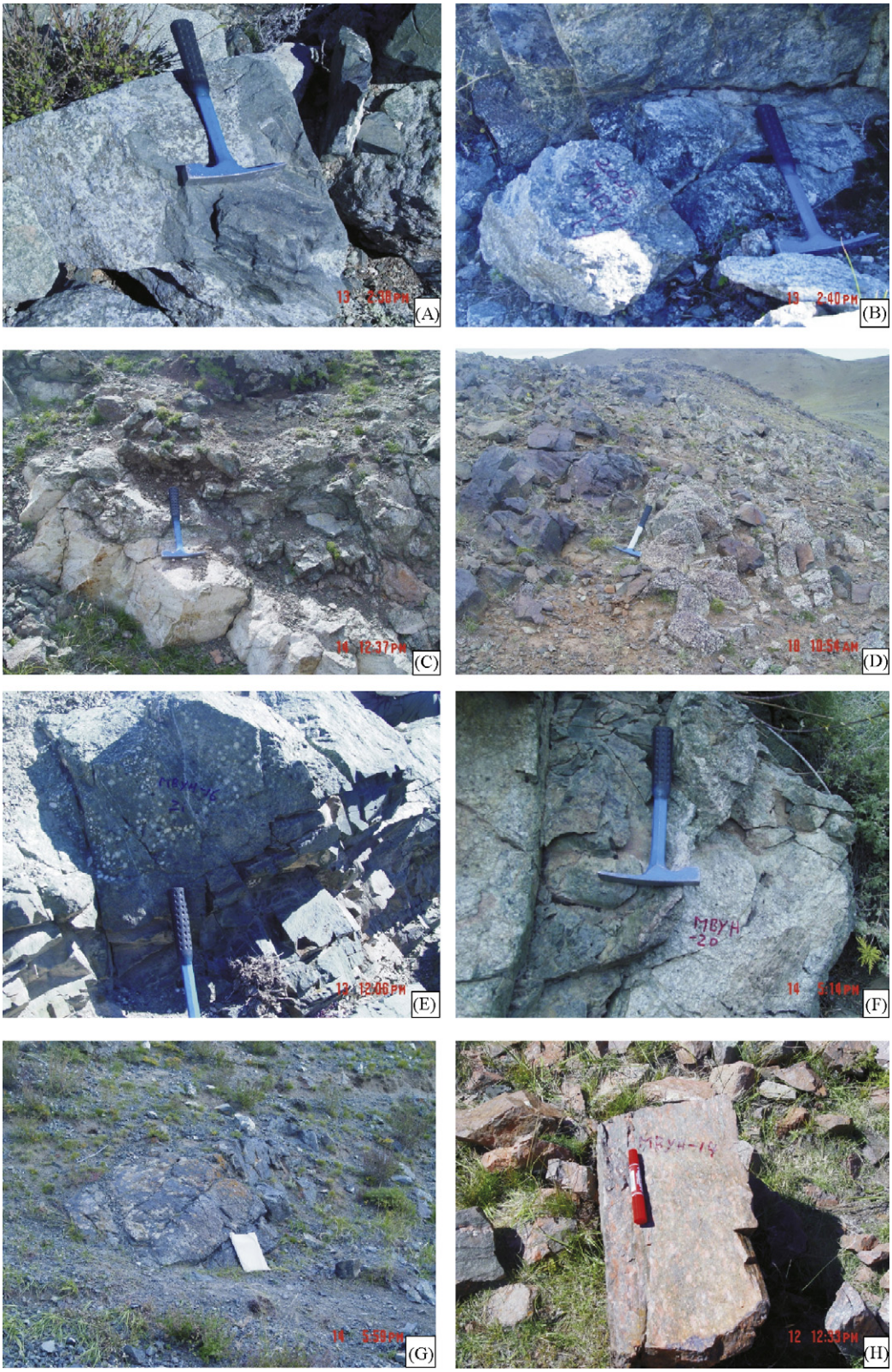

Fig. 3. Photographs showing field relationships of representative samples. (A) Garnet-rich rodingite containing a xenolith of pyroxenite; (B) Rodingite (MBYH17-1) grading into layered gabbro; (C) Isotropic amphibole gabbro (MBYH18-1) and plagiogranite (MBYH18-2); (D) Coarse-grained gabbro (MBYH08-1) and diabase dike (MBYH08-2); (E) Plagiophyric (MBYH16-1) and aphyric dikes; (F) Plagiophyric (MBYH20-1) and aphyric (MBYH20-2) dikes; (G) Porphyritic gabbro (MBYH22) occurring in basalt; and (H) Syenite porphyry (MBYH14).

Institute of Geology, Chinese Academy of Geological Sciences, Beijing, using conventional column chemistry and a TIMS (MAT 261). $^{143}Nd/^{144}Nd$ ratios were corrected for mass fractionation relative to $^{146}Nd/^{144}Nd = 0.7219$ and are reported with reference to the La Jolla Nd standard = 0.511860. Mass fractionation correction for $^{87}Sr/^{86}Sr$ is relative to $^{86}Sr/^{88}Sr = 0.1194$. Table 1 summarizes the geological, geochemical, and age data of all analyzed samples. Major and trace element contents are given in Table 2, and the Nd and Sr isotopic data in Table 3. Initial ε_{Nd} values and $^{87}Sr/^{86}Sr$ ratios were calculated for magmatic ages as determined from SHRIMP zircon analyses.

4.1. Rodingite, coarse-grained gabbro, amphibole gabbro and plagiogranite

Rodingite sample MBYH17-1 (for composition, see Table 2) has a high Al_2O_3 content, reflecting a high model content of plagioclase in its layered gabbro protolith (see Section 3.1.1). The rock has a low total REE abundance and displays a pronounced positive Eu-anomaly in the chondrite-normalized REE pattern (Fig. 4A), coupled with a strong positive Sr-anomaly in a primitive mantle-normalized trace element variation diagram (Fig. 4B). Although the sample is highly metasomatized, these geochemical features are consistent with plagioclase accumulation of a cumulate gabbro protolith. The ε_{Nd} (t = 647 Ma) value (7.6; Table 3) plots well above the depleted mantle evolution curve (not shown; see Nelson and DePaolo, 1984) and is quite close to the modern NMORB range (ε_{Nd} = 8–12; McCulloch and Cameron, 1983). The initial $^{87}Sr/^{86}Sr$ ratio (0.70257) is comparable to that of modern NMORB value (average $^{87}Sr/^{86}Sr = 0.7025$; McCulloch and Perfit, 1981). We thus suggest that the rodingite protolith (layered gabbro) originated from a NMORB magma. Metasomatism appears to have had a minimal impact on the Nd–Sr isotopic system.

Coarse-grained gabbro sample MBYH08-1 (Table 2) has a slightly lower Al_2O_3 content than the rodingite. The total REE abundance is low, and the positive Eu- and Sr-anomalies indicative of plagioclase accumulation are pronounced (Fig. 4A and B). These two samples are gabbroic cumulates and probably come from the lower part of the ophiolite complex.

Amphibole gabbro sample MBYH18-1 (Table 2) is more evolved than the gabbroic cumulates; this is clearly shown by its high total REE content and relatively high TiO_2 and TFe_2O_3 concentrations. The negligible positive Eu- (Fig. 4A) and Sr- (Fig. 4B) anomalies imply insignificant accumulation of plagioclase. Hence, this amphibole gabbro may represent a slowly cooled magma that characterizes high-level gabbros of many ophiolites (e.g. Coogan et al., 2002; Lissenberg et al., 2004). The nearby serpentinite sample MBYH19 is an altered harzburgite (Table 2), which has extremely high Cr (5275 ppm) and Ni (1544 ppm) contents suggestive of a residual mantle origin.

Plagiogranite sample MBYH18-2 (Table 2) is low in K_2O, in common with oceanic plagiogranites (e.g. Coleman and Peterman, 1975), and plots as oceanic ridge granite (ORG) in the Rb versus Y + Nb diagram of Pearce et al. (1984) (not shown). The negative Eu-anomaly indicates plagioclase fractionation prior to crystallization (Fig. 4A).

There is an overall increase in REE concentration level from the gabbroic cumulates through high-level gabbros to plagiogranite. This, together with their similar, more or less LREE-enriched patterns (Fig. 4A), suggests that these rocks are differentiates of an evolving magma that generated the Bayankhongor oceanic crust. The initial ε_{Nd} values (+7.6 to +4.7) and $^{87}Sr/^{86}Sr$ ratios (0.70279–0.70327) (Table 3) are confined to the depleted mantle range (Nelson and DePaolo, 1984) that dates back to the late Neoproterozoic (ca. 655–636 Ma).

Table 1
Summary of geological, geochemical and SHRIMP age data.

Unit/sample no.	Location	Lithology	Field occurrence	Geochemical interpretation	Age	Tectonic setting
Bayankhongor ophiolite						
MBYH18-2	46°38′12.9N, 99°33′43.8E	Plagiogranite	Thick (ca. 0.8 m) band within amphibole gabbro	Oceanic ridge granite	636 ± 6 Ma; n = 12, χ^2 = 0.95	Spreading ridge
MBYH18-1		Amphibole gabbro	Gabbro massif	High-level gabbro	647 ± 7 Ma; n = 15, χ^2 = 0.52	
MBYH08-1	46°06′34.2N, 100° 35′01E	Gabbro	Gabbro massif		640 ± 5 Ma; n = 12, χ^2 = 2. 92	
MBYH17-1	46°46′41.1N, 99° 15′35.746 E	Rodingite	Associated with and transitional to layered gabbro	Cumulate	647 ± 6 Ma; n = 14, χ^2 = 1.73	
Unnumbered*	46°43.233′N, 99°17.274′E	Anorthosite	Small lenses within layered gabbro		655 ± 4 Ma; n = 17, χ^2 = 0.49	
Early Paleozoic intrusions						
M9901**	46°21.81′ N; 99°44.36′E	Granite	Intrusion in Burd Gol mélange	High-K calc-alkaline	514 ± 10 Ma; n = 14	Continental margin
MBYH14	46°44′48.7N, 99° 07′37.7E	Syenite porphyry	Intrusion in Burd Gol mélange	Shoshonitic	523 ± 4 Ma; n = 9, χ^2 = 2.2	
Dikes, porphoryric gabbro and pillow basalt						
MBYH17-2	46°46′41.1N, 99° 15′35.746 E	Leucogabbro	Dike cut gabbro	Broadly asthenospheric mantle-derived rocks	298 ± 2 Ma; n = 12, χ^2 = 2.32	Intra-continental rift
MBYH 16-1	46°43′54.3N, 99°18′10.5E	Plagiophyric dike	"Sheeted dikes"		231 ± 4 Ma; n = 2, χ^2 = 0.58	
MBYH 20-1	46°30′16.1N, 99°56′30.9E	Plagiophyric dike			218 ± 9 Ma; n = 2, χ^2 = 0.18	
MBYH20-2		Aphyric dike			Youngest zircon ca. 238 Ma	
MBYH08-2	46°06′34.2N, 100° 35′01E	Diabase	Dike cut gabbro		210 ± 5 Ma; n = 3, χ^2 = 0.77	
MBYH22	46° 30′ 28.7N, 99° 55′ 18.1E	Porphyritic gabbro			237 ± 2 Ma; n = 8, χ^2 = 4.24	
MBYH21	46°30′ 34.6N; 99° 55′ 22.2E	Pillow basalt				

* Recalculated from Kovach et al. (2005).
** After Jahn et al. (2004).

Table 2
Major and trace element compositions of analyzed samples.

Sample	Serpentinite	Samples from gabbro massif				Dikes				Pillow basalt	Porphoryric gabbro	Syeniteporphyry
	MBYH19	Gabbro MBYH18-1	Plagiogranite MBYH18-2	Gabbro MBYH08-1	Rodingite MBYH17-1	Leucogabbro dike MBYH17-2	Plagiophyric dike MBYH16-1	Aphyric dike MBYH20-2	Diabase MBYH08-2	MBYH21	MBYH22	MBYH14
Oxides (%)												
SiO_2	38.65	50.32	66.88	49.1	48.06	48.34	48.74	50.36	50.37	49.6	48.88	57.28
TiO_2	0.04	1.02	0.26	0.26	0.18	0.13	0.71	2.23	1.15	1.51	0.38	0.79
Al_2O_3	1.16	16.13	18.14	17.32	20.75	25.15	21.58	13.31	14.59	13.5	15.05	19.48
TFe_2O_3	10.41	7.63	1.3	4.91	5.14	2.89	5.9	11.71	9.87	12.06	7.08	5.1
MnO	0.08	0.13	0.02	0.09	0.09	0.05	0.08	0.18	0.16	0.19	0.09	0.08
MgO	37.3	7.64	0.32	9.25	7	3.69	3.18	7.07	7.88	7.4	10.11	2.18
CaO	0.18	10.53	1.49	14.63	13.88	14.28	12.02	7.95	11.17	9.62	12.64	3.62
Na_2O	0.05	2.09	10.89	0.69	1.09	1.82	3.09	3.83	2	3.17	1.66	4.35
K_2O	0.04	0.95	0.09	0.1	0.08	0.005	0.49	0.09	0.33	0.22	0.39	5.07
P_2O_5	0.01	0.08	0.07	0.39	0.01	0.01	0.08	0.35	0.11	0.14	0.02	0.28
LOI	11.58	3.12	0.46	2.84	3.33	3.1	3.79	2.79	2.26	2.1	3.23	1.41
TOL	99.5	99.64	99.92	99.58	99.61	99.51	99.66	99.87	99.89	99.51	99.53	99.64
REE ($\times 10^{-6}$)												
La	0.4	9.13	13	1.58	2.88	1.41	6.21	13.8	6.3	4.81	1.79	117
Ce	1.21	21.1	34.8	4.14	6.38	3.4	13.7	34.5	16.2	13.1	4.62	223
Pr	0.29	2.93	4.29	0.72	0.93	0.57	1.84	4.85	2.46	2.12	0.77	23.5
Nd	0.79	13.7	16.9	3.17	3.87	2.22	8	24.2	12.4	11.1	3.49	86
Sm	0.033	3.44	3.14	0.8	0.91	0.44	1.88	7.05	3.68	3.68	1.01	12.8
Eu	0.084	1.47	0.75	0.45	0.47	0.39	0.72	2.28	1.35	1.25	0.66	3.43
Gd	0.1	3.92	3.02	1.11	1.18	0.62	2.22	8.85	4.75	5.04	1.49	10.2
Tb	0.025	0.67	0.48	0.2	0.23	0.11	0.38	1.57	0.86	0.95	0.28	1.25
Dy	0.039	3.95	2.77	1.2	1.34	0.6	2.22	10	5.5	6.16	1.77	6.29
Ho	0.02	0.82	0.61	0.27	0.29	0.14	0.47	2.15	1.18	1.37	0.39	1.14
Er	0.044	2.3	1.91	0.73	0.86	0.37	1.35	6.26	3.42	4	1.09	3.05
Tm	0.012	0.34	0.32	0.11	0.14	0.06	0.21	0.94	0.51	0.6	0.16	0.43
Yb	0.07	2.03	2.08	0.63	0.82	0.34	1.25	5.66	3.1	3.68	0.97	2.46
Lu	0.0059	0.3	0.37	1.58	0.12	0.044	0.18	0.89	0.47	0.57	0.15	0.38
Y	0.59	20.8	18.2	6.24	8.32	3.75	13.6	58	30.4	37.1	10.2	28.6
Trace elements ($\times 10^{-6}$)												
Sc	6.77	40.5	2.9	33.5	28.9	16	18.1	37.5	40.9	46.6	37.9	9.96
V	40.2	170	35.5	145	113	91	144	272	231	312	158	76.8
Cr	5275	142	4.27	541	301	44.4	45.6	67.6	151	41	349	32.2
Co	125	38.2	2.41	27.7	32.5	12.5	21.3	36.4	38.7	47.2	37.8	11
Ni	1544	67.4	12.1	164	81.3	31.1	29.3	32.8	80.4	41	143	19.6
Cu	45.9	68.8	6.8	46.6	38	34.2	44.9	14.4	62.8	57.7	16.4	5.49
Zn	66.7	57.2	9.29	27.4	26.9	13.3	33.1	66.9	63.7	70.2	19.5	71.3
Ga	2.06	16.7	25.3	10.2	13.2	12.9	15.7	18.6	15.5	17.3	12.5	23.6
Rb	0.21	24	1.76	1.64	1.68	0.87	10.8	5.07	7.4	3.19	6.05	152
Sr	5.61	346	126	246	282	316	196	130	162	132	87.9	873
Zr	3.1	52.1	376	9.43	12.7	9.15	50.2	199	94.1	94.9	13.8	481
Nb	0.49	12.7	32.2	0.84	3.02	1.18	10.4	17.8	7.73	5.58	1.29	15.8
Ta	0.016	0.78	3.99	0.061	0.31	0.072	0.59	1.16	0.54	0.35	0.074	0.9
Cs	0.059	0.62	0.054	0.077	0.25	0.078	0.17	0.54	0.15	0.23	0.22	3.02
Ba	5.13	167	49	28.3	46.9	30.3	165	33.1	101	48.4	49.2	2354
Hf	0.031	1.59	10.3	0.32	0.46	0.21	1.21	5.35	2.72	2.62	0.43	11.6
Pb	0.68	5.52	2.28	1.11	0.99	0.87	1.03	2.87	1.12	0.9	0.74	25.8
Th	0.018	0.91	14	0.092	0.78	0.16	0.58	1.43	0.63	0.52	0.046	20.4
U	0.063	0.17	1.31	0.13	0.1	0.039	0.14	0.45	0.17	0.14	0.045	1.76

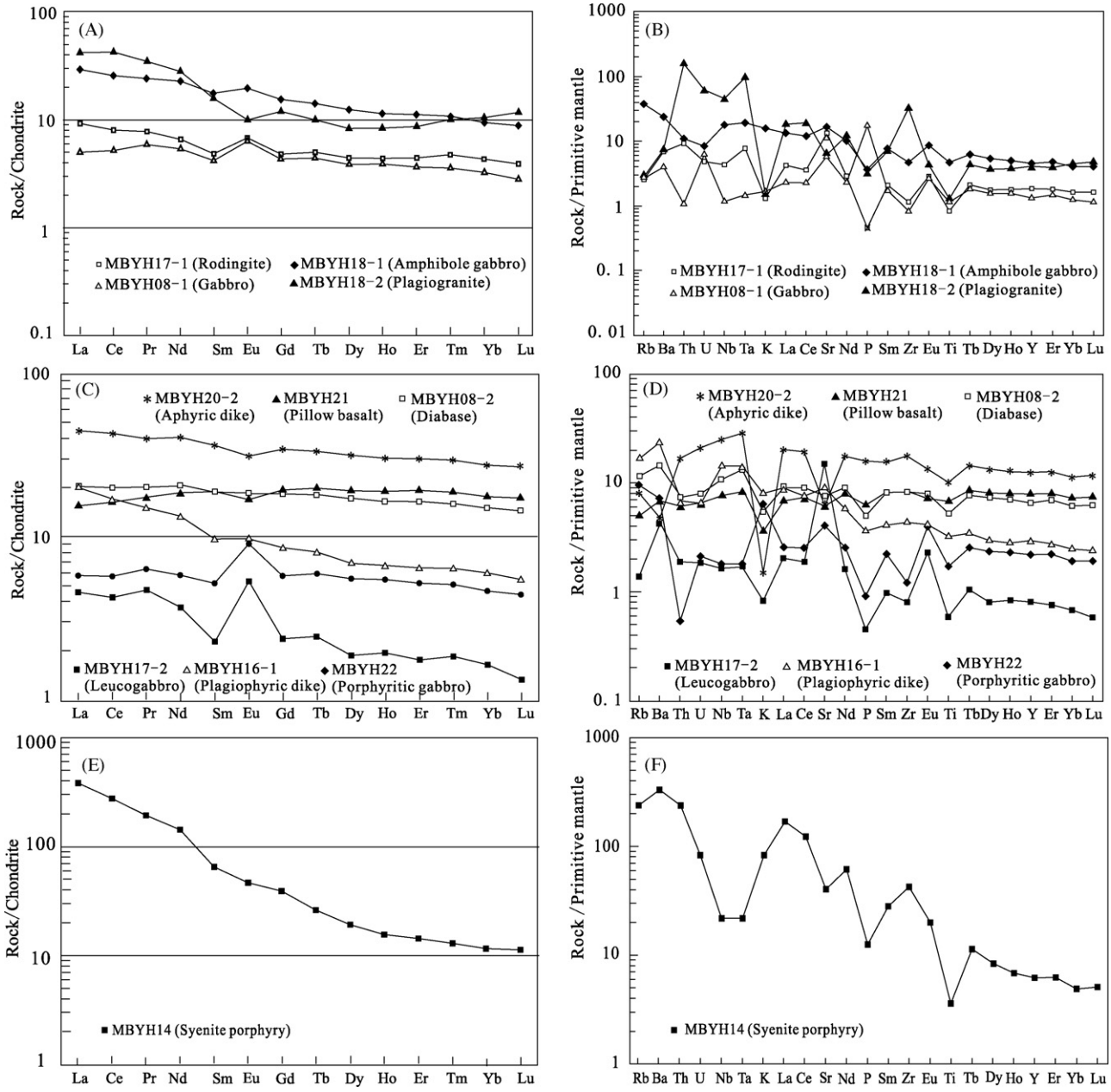

Fig. 4. Chondrite-normalized REE patterns (left) and multi-element variation diagrams (right). (A and B) Rodingite (MBYH17-1), coarse-grained gabbro (MBYH08-1), amphibole gabbro (MBYH18-1), plagiogranite (MBYH18-2) and harzburgite (MBYH19). (C) and (D) Leucogabbro dike (MBYH17-2), "sheeted" dikes (MBYH16-1, MBYH20-2), diabase dike (MBYH18-2), porphyritic gabbro (MBYH22) and pillow basalt (MBYH21). (E and F): Syenite porphyry (MBYH14). Chondrite values after Masuda et al. (1973); Primitive mantle values after Hofmann (1988).

4.2. Leucogabbro dike, "sheeted dikes", diabase dike and porphyritic gabbro

Leucogabbro dike sample MBYH17-2 (Table 2) has high Al_2O_3 and CaO, and low TFe_2O_3 and MgO contents and a strong positive Eu-anomaly indicative of plagioclase accumulation (Fig. 4C). The $\varepsilon_{Nd(t)}$ value is +9.2, and the initial $^{87}Sr/^{86}Sr$ ratio is 0.70275 (Table 3).

MBYH 16-1 and MBYH20-2 are "sheeted" dike samples. The plagiophyric dike (MBYH16-1) (Table 2) exhibits a sloping REE pattern ($La_n/Yb_n = 3$) (Fig. 4C), whereas the aphyric dike (MBYH20-2) has a nearly flat pattern ($La_n/Yb_n = 1.5$) (Fig. 4C). The aphyric dike has higher TiO_2 (2.2%), total REE ($La_n = 36.5$), and $\varepsilon_{Nd(t)}$ value (+9.6) (Table 3) than the plagiophyric dike ($TiO_2 = 0.7\%$; $La_n = 16.4$; $\varepsilon_{Nd(t)} = +5.1$).

Diabase dike sample MBYH08-2 (Table 2) shows a nearly flat REE pattern ($La_n/Yb_n = 1.2$; $La_n = 16.7$) (Fig. 4C) and is similar in composition to basaltic pillow lava sample MBYH21, but the latter is slightly LREE-depleted ($La_n/Yb_n = 0.8$; $La_n = 12.7$). Their $\varepsilon_{Nd(t)}$ values and initial $^{87}Sr/^{86}Sr$ ratios are +7.8 and 0.70363 for the diabase, and +12.3 and 0.70303 for the pillow lava, respectively (Table 3).

Porphyritic gabbro sample MBYH22 (Table 2) is compositionally primitive with high MgO, Cr and Ni contents. The REE pattern (Fig. 4C) shows a strong positive Eu-anomaly, consistent with high modal plagioclase content. This sample has an $\varepsilon_{Nd(t)}$ value of +9.6 and an initial $^{87}Sr/^{86}Sr$ ratio of 0.70353.

Using a TAS diagram (Le Bas et al., 1986) (not shown) the analyzed "sheeted dikes", diabase dike and pillow lava are classified

Table 3
Nd–Sr isotopic data of Bayankhongor samples.

Sample no.	Lithology	Age (Ma) Zircon	[Rb] (ppm)	[Sr] (ppm)	$^{87}Rb/^{86}Sr$	$^{87}Sr/^{86}Sr$	±2sm	I (Sr)	[Sm] (ppm)	[Nd] (ppm)	$^{147}Sm/^{144}Nd$	$^{143}Nd/^{144}Nd$	±2sm	$\varepsilon_{Nd(0)}$	$\varepsilon_{Nd(t)}$	F (Sm/Nd)	T_{DM}-1 (Ma)
MBYH18-1	Amphibole gabbro	647	14.8	250	0.172	0.704853	15	0.703272.43		10.4	0.1413	0.512795	8	3.1	7.6	−0.28	748
MBYH18-2	Plagiogranite	636	1.34	105.2	0.037	0.703195	13	0.702862.95		15.38	0.1161	0.512544	12	−1.8	4.7	−0.41	946
MBYH08-1	Gabbro	640	1.01	161	0.018	0.702958	12	0.702790.535		1.68	0.1933	0.512873	10	4.6	4.9	−0.02	2062
MBYH17-1	Rodingite	647	1.08	231.5	0.013	0.702696	15	0.702570.645		2.63	0.148	0.512823	15	3.6	7.6	−0.25	759
MBYH17-2	Leucogabbro dike	298	4.77	214.9	0.006	0.702779	14	0.702750.255		2.43	0.0635	0.512852	16	4.2	9.2	−0.68	303
MBYH16-1	Plagiophyric dike	231							1.43	6.51	0.1324	0.512803	10	3.2	5.1	−0.33	651
MBYH20-2	Aphyric dike	238	3.15	103.2	0.088	0.702937	13	0.702645.18		19.47	0.1609	0.513075	7	8.5	9.6	−0.18	217
MBYH08-2	Diabase	210	5.08	135	0.122	0.703996	11	0.703632.76		10.75	0.1555	0.512981	6	6.7	7.8	−0.21	443
MBYH21	Basalt	220	1.55	97.9	0.046	0.703169	11	0.703033.1		9.02	0.2077	0.513266	8	12.3	11.9	0.06	−2986
MBYH22	Porphyritic gabbro	237	3.82	64.1	0.173	0.704108	14	0.703530.819		2.35	0.2104	0.513153	10	10	9.6	0.07	−141

as tholeiitic basalt. Their primitive mantle-normalized trace element variation diagrams (Fig. 4D) show positive Nb–Ta anomalies with reference to Th (K) and La that differ from MORB. These rocks, together with the leucogabbro dike and the porphyritic gabbro, all have medium to high positive $\varepsilon_{Nd(t)}$ values (+12.3 to +5.1) and low initial $^{87}Sr/^{86}Sr$ ratios (0.7026–0.7036). The isotopic compositions suggest a more depleted mantle source ($^{87}Sr/^{86}Sr = 0.7030$; Menzies et al., 1991; Peters et al., 2008) than that of the Bayankhongor ophiolite ($\varepsilon_{Nd} = +7.6$ to +4.7).

4.3. Syenite porphyry

Syenite porphyry sample MBYH14 (Table 2) is low in TiO_2 (0.8%), and high in K_2O/Na_2O (>1) and Al_2O_3 (19.5%); we interpret it to have a shoshonite affinity based on the K_2O versus SiO_2 diagram (Le Maitre et al., 1989) (not shown). It is enriched in Rb (152 ppm), Sr (873 ppm), Ba (2354 ppm), Th (20.4 ppm) (Fig. 4F) and LREE ($La_n = 310$; $La_n/Yb_n = 32$; Fig. 4E), in accord with the shoshonite association (Morrison, 1980). This rock displays pronounced Nb–Ta–Ti anomalies (Fig. 4F), suggesting a subduction component, either from subarc mantle wedge (e.g. Morrison, 1980) or from a subduction-enriched subcontinental lithospheric mantle (Turner et al., 1996). The high Ce/Yb ratio (9:1) is a geochemical argument for a continental setting (Gill et al., 2004). This is consistent with the fact that the syenite porphyry intruded the boundary between the Southern Volcanic Belt and the Burd Gol mélange. Generally, rocks of the shoshonite association generated in continental settings (post-subduction, post-collisional) have Ce/Yb rations >45, whereas those of oceanic island arcs have Ce/Yb rations less than 45 (Gill et al., 2004).

5. Zircon ages

Zircon cathodoluminescence (CL) images are shown in Fig. 5. Isotopic analyses were performed on the SHRIMP II in Beijing, and analytical procedures are given by Williams et al. (1996). Each measurement consisted of five scans through Zr, Pb, U and Th species of interest analyzed on a single electronic multiplier by cyclic stepping of the magnetic field. The PRAWN data reduction software (see Williams et al., 1996) was used for data processing, and ages were calculated using the constants recommended by Steiger and Jäger (1977). Common Pb corrections were based on the measured $^{204}Pb/^{206}Pb$ or $^{208}Pb/^{206}Pb$ ratios as described in Compston et al. (1992), and initial Pb compositions were listed by Cumming and Richards (1975). Errors for individual analyses are given at the 1-sigma level in the supplementary Table S1, and were determined solely from counting statistics. Unless otherwise stated, all ages reported in the text are weighted mean concordant $^{206}Pb/^{238}U$ ages (uncertainties are given at the 95% confidence limit). Chi-square (χ^2) was employed to test if an age population meets the statistical requirements. When $\chi^2 = 1$ for a large population, the error of the weighted mean age is consistent with the error of individual analyses, and there is no excess scatter (Black and Jagodzinski, 2003).

5.1. Rodingite, amphibole gabbro, plagiogranite and coarse-grained gabbro

5.1.1. Rodingite (MBYH17-1)

Zircons in this sample mostly display patchy and widely spaced zoning (Fig. 5A, left), a characteristic of gabbroic zircons (Corfu et al., 2003), but some grains (e.g. Fig. 5A, right) are internally homogeneous possibly indicating recrystallization during rodingitization. Most zircons have low uranium contents (26–60 ppm; Table S1) and discordant isotopic compositions. On a Concordia diagram (Fig. 6A), all data are indistinguishable and define a weighted mean

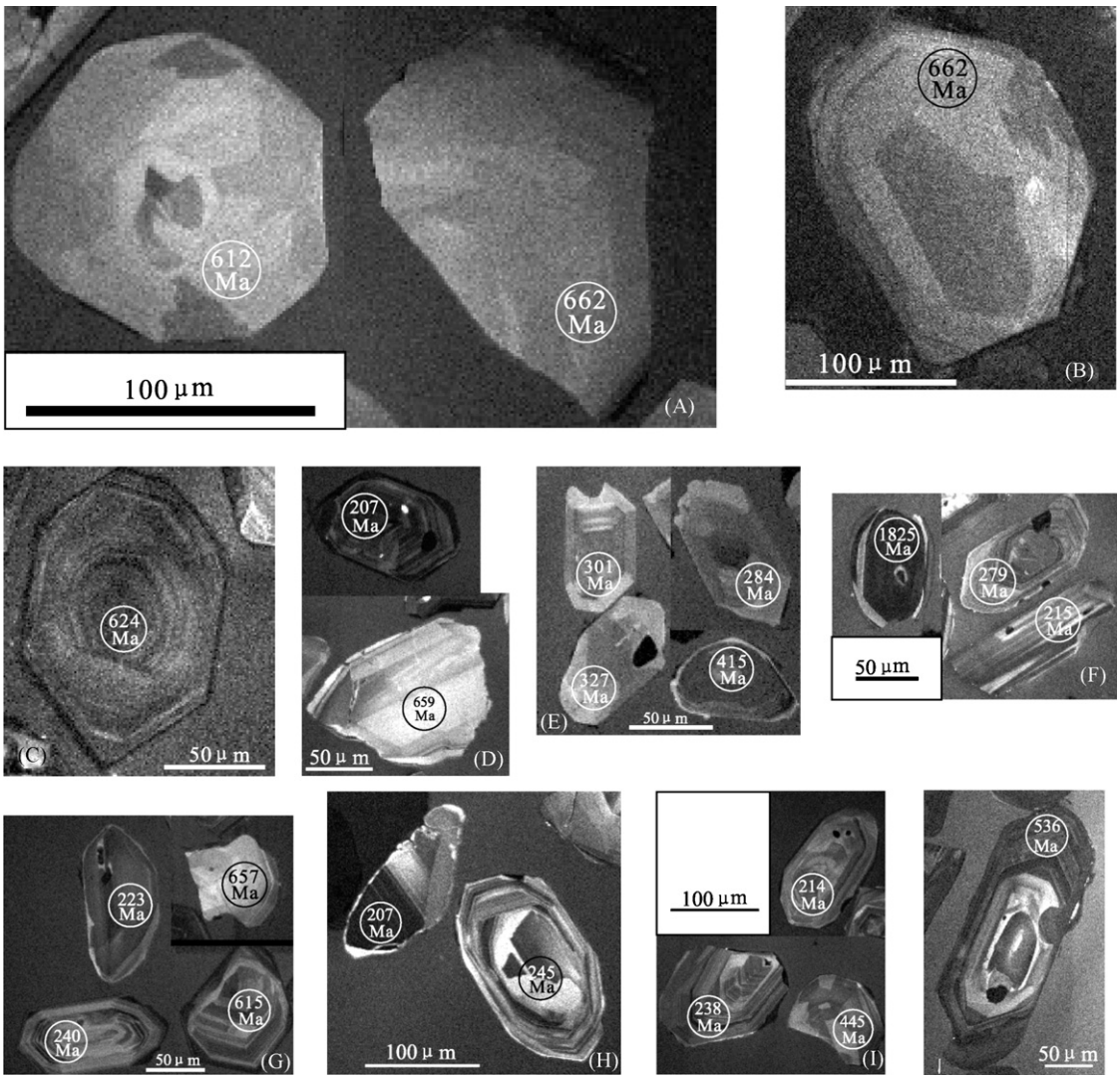

Fig. 5. Representative CL images of zircons. (A) Rodingite (MBYH17-1); (B) Amphibole gabbro (MBYH18-1); (C) Plagiogranite (MBYH18-2); (D) coarse-grained isotropic gabbro (MBYH08-1); (E) Leucogabbro dike (MBYH17-2); (F) Plagiophyric dike (MBYH16-1); (G) Plagiophyric dike (MBYH20-1); (H) Diabase dike (MBYH08-2); (I) Porphyritic gabbro (MBYH22); (J) Syenite porphyry (MBYH14).

$^{206}Pb/^{238}U$ age of 647 ± 6 Ma (n = 14, χ^2 = 1.73). The discordance of isotopic compositions is most likely attributable to rodingitization that disturbed the zircon U–Pb system, and we interpret 647 ± 6 Ma as a minimum age for the time of crystallization of the layered gabbro, the protolith of the rodingite.

This age is similar to that of the previously dated anorthosite (Kovach et al., 2005) whose weighted mean age is recalculated here at 655 ± 4 Ma (n = 17, χ^2 = 0.49) (Fig. 6B, Table S1). In the previous data processing of Kovach et al. (2005) the uncertainties of individual analyses had been overestimated by involving additional error sources.

5.1.2. Amphibole gabbro (MBYH18-1) and plagiogranite (MBYH18-2)

The isotropic amphibole gabbro contains broadly zoned zircons that are also patchy (Fig. 5B). Fifteen analyses (Table S1) are concordantly clustered at 647 ± 7 Ma (χ^2 = 0.52) (Fig. 6C), which is interpreted as the crystallization age of the gabbro. Zircons from the plagiogranite are simple, oscillatory zoned, magmatic crystals (Fig. 5C). The crystallization age, as determined from 12 analyses, is 636 ± 6 Ma (χ^2 = 0.95) (Fig. 6D).

5.1.3. Coarse-grained gabbro with mafic and felsic veins (MBYH08-1)

Zircons in this sample are heterogeneous in appearance and in CL images. The dominant population (60%) has irregular shapes with patches, stripes and broadly spaced zoning (e.g. Fig. 5D, bottom). A few grains are prismatic and rythmically zoned (e.g. Fig. 5D, top), whereas other zircons are more or less rounded. In Fig. 6E, all isotopic compositions (Table S1) are near-concordant, and the dominant zircons are grouped at 640 ± 5 Ma (n = 12, χ^2 = 2.92). This age is similar to, but slightly younger than, that of other gabbroic samples. A possible reason for this is that the U–Pb system may have been disturbed by late-stage thermal events.

Two prismatic, rhythmically zoned crystals have distinctly younger ages (ca. 194–214 Ma), and the remaining analyses are either clustered at 270 ± 2 Ma (n = 8, χ^2 = 2.79; Fig. 6E) or dispersed along Concordia from ca. 750 to 950 Ma. We consider that the gabbro was intruded by veins in the Permo–Triassic, at which time the zircon xenocrysts (ca. 750–950 Ma) may have been captured. This is supported by the fact that the dated gabbro contains pervasive mafic and felsic veins.

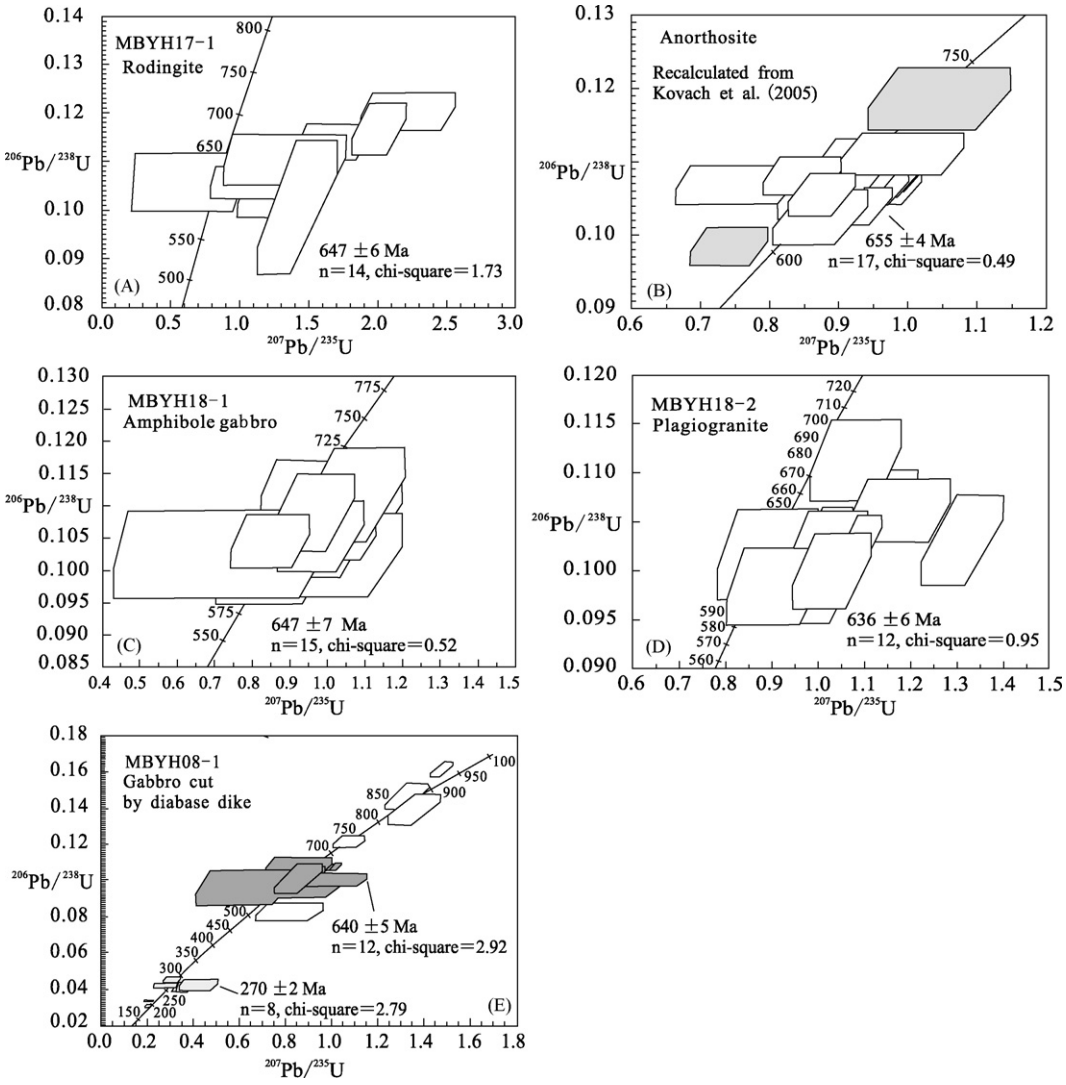

Fig. 6. Concordia diagrams. (A) Rodingite (MBYH17-1); (B) Anorthosite (recalculated from raw data of Kovach et al., 2005). Dark grey marks two analytical exceptions; (C) Amphibole gabbro (MBYH18-1); (D) Plagiogranite (MBYH18-2); (E) Coarse-grained gabbro (MBYH08-1). Dark grey marks gabbroic zircons and light grey denotes a younger age group.

5.1.4. Summary

The above results demonstrate that the gabbroic cumulates (anorthosite, 655 ± 4 Ma; metasomatised layered gabbro-rodingite, 647 ± 6 Ma) are the oldest rocks, followed by high-level isotropic gabbro (amphibole gabbro, 647 ± 7 Ma), and plagiogranite (636 ± 6 Ma), the youngest. This age relationship is consistent with the idealized plutonic sequence of an ophiolite (e.g. Boudier et al., 1996; Kelemen and Aharonov, 1998; Nicolas, 1989) that evolved within ca. 20 Ma. Also, the Neoproterozoic gabbro was intruded by veins of Permo–Triassic age, which entrained some Neoproterozoic zircon xenocrysts.

5.2. Leucogabbro dike, "sheeted dikes", diabase dike and porphyritic gabbro

5.2.1. Leucogabbro dike (MBYH17-2)

This sample contains mostly small (<50 μm) prismatic zircons with patches of different contrast in CL (Fig. 5E). Their U–Pb isotopic compositions (Table S1) are concordant or near concordant, and the weighted mean age is 298 ± 2 Ma (n = 8, χ^2 = 2.32) (Fig. 7A). A few zircons have rounded shapes (e.g. Fig. 5E, lower right) and older ages (ca. 354–466 Ma) and are interpreted as xenocrysts.

5.2.2. "Sheeted dikes" (MBYH16-1, MBYH20-1 and MBYH20-2)

Plagiophyric basaltic dike sample MBYH16-1 contains two zircon populations with Paleoproterozoic and Paleozoic-early Mesozoic ages. Three Paleoproterozoic zircons are well rounded (e.g. Fig. 5F, left), and their $^{207}Pb/^{206}Pb$ ages range from 1772 to 1825 Ma (Table S1). The Paleozoic–early Mesozoic population (487–215 Ma) is characterized by a wide scatter of individual ages over a ca. 270 Ma range. The two youngest zircons define a mean age of 231 ± 4 Ma (Fig. 7B).

Plagiophyric dike sample MBYH20-1 exhibits a similar age scatter (ca. 215–494 Ma, Table S1), in which the two youngest analyses (e.g. Fig. 5G, upper left) combine to give a mean age of 218 ± 9 Ma. This sample also contains ca. 595–647 Ma zircons (weighted mean age is 638 ± 9 Ma, n = 6, χ^2 = 0.94; Fig. 7C), either internally homogeneous or rhythmically zoned (Fig. 5G, right). Two tiny zircon grains (<50 μm) from aphyric dike sample MBYH20-2 yielded apparent $^{206}Pb/^{238}U$ ages of 239 ± 12 Ma and 283 ±26 Ma (Table S1, Fig. 7D).

5.2.3. Isolated diabase dike (MBYH08-2) in gabbro

Zircons in this sample mostly have discordant isotopic compositions (Table S1, Fig. 7E), and their ages are spread from ca. 199

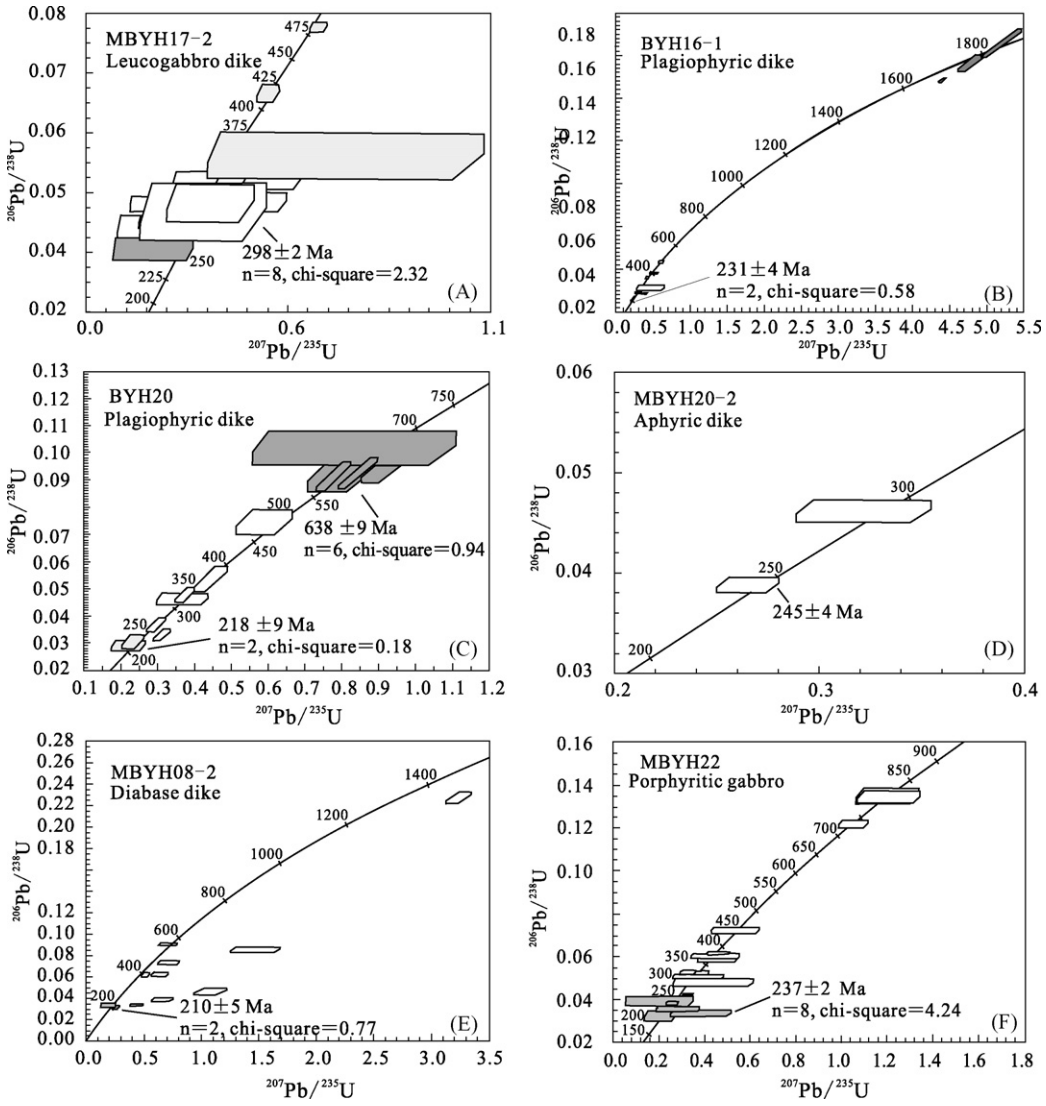

Fig. 7. Concordia diagrams. (A) Leucogabbro dike (MBYH17-2). Light grey marks xenocrysts and dark grey denotes analytical exception; (B) Plagiophyric dike (MBYH16-1). Dark grey marks Palaeoproterozoic xenocrysts; (C) Plagiophyric dike (MBYH20-1). Dark grey marks the late Neoproterozoic age group; (D) Aphyric dike (MBYH20-2); (E) Diabase dike (MBYH08-2); (F) Porphyritic gabbro (MBYH22). Dark grey marks the youngest age group.

to 1336 Ma. However, the two youngest, concordant grains (e.g. Fig. 5H, left) have the same $^{206}Pb/^{238}U$ age within error, and the mean age is given at 210 ± 5 Ma (n = 2, χ^2 = 0.77).

5.2.4. Porphyritic gabbro (MBYH22)

Most zircons (ca. 80%) display rhythmic growth zoning under CL (Fig. 5I, top and left), but homogeneous and irregular zircon patterns are also present (Fig. 5I, right). Three zircons have $^{206}Pb/^{238}U$ ages in the range 734–808 Ma, ten in the range ca. 265–445 Ma, and eight in the range ca. 204–255 Ma. This youngest population defines a weighted mean age of 237 ± 2 Ma (n = 8, χ^2 = 4.22; Fig. 7F).

5.2.5. Summary

We interpret the youngest zircon age of each sample to represent the likely time of dike emplacement. These Permo–Triassic mafic rocks postdate the late Neoproterozoic ophiolite by ca. 340–430 Ma. The wide age spectrum in their xenocryst populations provides strong evidence for multiple source contamination. A reassessment of their tectonic setting is therefore given below (see Section 6.5).

5.3. Syenite porphyry

Zircons in sample MBYH14 are mostly prismatic with rhythmic zoning (Fig. 5J). Nine concordant analyses (Table S1) are grouped at 523 ± 2 Ma (χ^2 = 2.2) (Fig. 8), which is interpreted as the time of emplacement of the syenite porphyry. Three grains with irregular CL patterns have slightly older $^{206}Pb/^{238}U$ ages of 558–581 Ma and are interpreted as xenocrysts.

6. Discussion

6.1. Origin of the Bayankhongor ophiolite

The geochemical data and zircon ages reported above (Table 1) demonstrate that the Bayankhongor ophiolite was intruded and is overlain by late-stage intrusive and extrusive mafic rocks. This implies that at least part, if not all, of the tholeiitic basalts/dikes originally interpreted as part of the ophiolite are not related to the Neoproterozoic oceanic plutonic complex and, therefore, their geochemistry cannot be used to determine the tectonic setting of this ophiolite. Nevertheless, on the basis of our geochemical and geochronological data, a plutonic sequence of ophiolite can be rec-

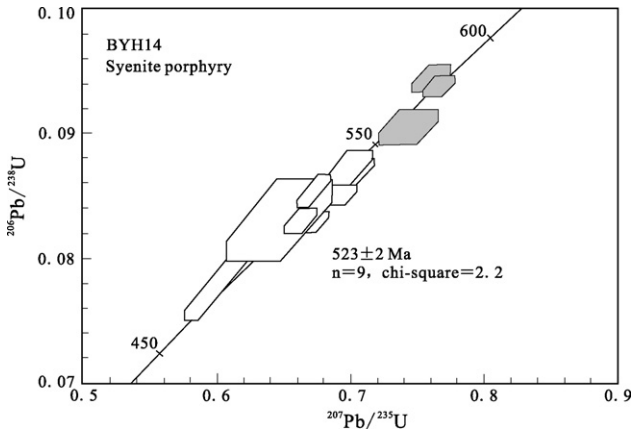

Fig. 8. Concordia diagrams of zircons from syenite porphyry (MBYH14). Dark grey marks inheritance.

ognized (Section 5.1.4). The Nd–Sr isotopic compositions (Table 3) point to a depleted mantle source, consistent with a mid-ocean-ridge origin.

Magmatic zircons of the plutonic sequence reflect a long time interval of ocean crust formation (ca. 20 Ma) from a gabbroic cumulate (655 ± 4 Ma to 647 ± 6 Ma), through high-level isotropic gabbro (647 ±7 Ma), to plagiogranite (636 ± 6 Ma) (Table 1). In contrast, many ophiolites such as the Coast Range of California (Hopson et al., 2008) and most Tethyan-type ophiolites (Wakabayashi and Dilek, 2003), show a short (generally 5 Ma or less) age range. The reason for this discrepancy is uncertain but, logically, the long duration of igneous formation implies a relatively wide oceanic basin or slow spreading.

6.2. Geological significance of the syenite porphyry

Buchan et al. (2001) suggested that the Burd Gol mélange was produced by subduction-accretion and represents an accretionary wedge, built up against the Baidrag microcontinent to the south. These authors also interpreted the South Volcanic Belt to the north (Figs. 1B and 2A) as an island arc. We concur that this scenario is realistic and that corresponding subduction was to the Northeast.

The Burd Gol mélange underwent Barrovian-type metamorphism, and is tectonically sandwiched between the South Volcanic Belt to the north and the Baidrag microcontinent to the south (Figs. 1B and 2A). Current geochronological information indicates that this mélange (metamorphism between 562 and 533 Ma; see Section 2.1.2) and the South Volcanic Belt (volcanism at ca. 544 Ma or earlier; see Section 2.1.3) evolved contemporaneously in late Neoproterozoic to earliest Cambrian times. Because of these spatial and temporal relationships, we consider that the three units form an arc-microcontinent collision zone and that the Barrovian-type metamorphism is linked to the collisional event.

The 523 ± 2 Ma syenite porphyry postdates the Barrovian-type metamorphism and thus the onset of arc-microcontinent collision. This rock occurs on the thrust boundary between the Burd Gol mélange and the South Volcanic Belt (Fig. 1B) and it is strongly foliated. It is therefore likely that the syenite porphyry was generated in a late collisional stage.

The 523 ± 2 Ma age for the syenite porphyry is similar to, but slightly older than, that of the high-K calc-alkaline granites (514 ± 10 Ma, Jahn et al., 2004). This is consistent with the common temporal relationship between syenite and granite in a typical syenite-granite suite, as generalized by Jahn et al. (2009) for the late Paleozoic, early Mesozoic and late Mesozoic syenite-granite suites in the Mongolian-Transbaikalian Belt which are part of the CAOB. These ages provide important time constraints on the transition from a compressional to an extensional environment. The syenite porphyry has a foliation, whereas the granites have not (Buchan et al., 2002; Jahn et al., 2004). This difference in deformation may suggest that the orogeny reached its terminal phase at ca. 523 Ma and that intra-continental plutonism occurred at ca. 514 Ma. Geochemically, the syenite porphyry has a shoshonitic affinity (see Section 4.3), and similar shoshonite-high-K calc-alkaline rock associations, considered as the magmatic expression of termination of orogeny, are well documented in the African–Eurasian suture zone in the Alps (e.g. Pamic et al., 2002) and in the Appalachians of Newfoundland (Whalen et al., 2006).

In central Mongolia, generation of the syenite porphyry was likely controlled by a subduction-enriched subcontinental lithospheric mantle and its overlying continental margin. The subduction signature is indicated by pronounced negative Nb–Ta–Ti anomalies; the subcontinental lithospheric mantle, which was the main magma source, is fingerprinted by high Ba–Sr contents (Table 2), and the continental margin is represented by the Burd Gol mélange. Therefore, the formation of the syenite porphyry during the terminal phase of orogeny was possibly triggered by slab breakoff. This process generally follows collision and allows upwelling of asthenosphere to partially melt the subduction-enriched subcontinental lithospheric mantle (Atherton and Ghani, 2002; Davies and von Blanckenburg, 1995; Whalen et al., 2006).

6.3. Post-sea floor spreading evolution of the ophiolite

As discussed earlier, the Bayankhongor oceanic crust formed as early as ca. 655–636 Ma; however, the central Mongolian region reached its terminal orogenic phase as late as ca. 523 Ma. The Delb Khairkhan mélange contains material, for example, arc lavas (Buchan, 2002), from the South Volcanic Belt, as well as from the Bayankhongor ophiolite (Buchan et al., 2001). This demonstrates that arrival of the ocean floor at the trench and incorporation of the oceanic crust into the accretionary wedge occurred after arc volcanism (ca. 544 Ma). Thus, the ophiolite apparently experienced at least 92 Ma (636–544 Ma) of drift in the ocean prior to its accretion to the orogenic belt.

Previously, there has been agreement on the stratigraphy of the Bayankhongor ophiolite (see Tomurtogoo et al., 2006, for review). By such consideration, all igneous rocks in the serpentinite mélange, i.e., ultramafic rocks, gabbros, sheeted dikes and lava flows were combined to fit an idealized ophiolite stratigraphy. Kovach et al. (2005) and Tomurtogoo et al. (2006) also recognized alkaline and tholeiitic lavas but erroneously suggested a geochemical unity with the ophiolite. It is now clear that the ophiolite mélange includes at least three distinctive igneous formations: (1) a late Neoproterozoic (ca. 655–636 Ma; Table 1) fragmented ophiolite; (2) (Cambrian and earlier) alkaline lavas (Kovach et al., 2005; Tomurtogoo et al., 2006) that postdate sea-floor spreading; and (3) Permo–Triassic tholeiitic dikes and lavas (Table 1). We now discuss the tectonic implications of the alkaline lavas and Permo–Triassic mafic rocks (see Section 6.5).

The presence of alkaline lavas within the ophiolite mélange suggests derivation from a seamount, volcanic island or oceanic plateau within the ocean, as documented in the Northland ophiolite, New Zealand (Malpas et al., 1992), the Masirah island ophiolite of Oman (Meyer et al., 1996), and the obducted Cretaceous terranes in western Colombia and the Caribbean (Kerr et al., 1998). Kovach et al. (2005) interpreted the Bayankhongor magmatic suite to represent an oceanic plateau, based on analogous geochemical features of the Bayankhongor lavas with those of the Ontong Java and Caribbean–Columbian plateaus. Buchan et al. (2001) identified seamount blocks of lower Cambrian age in the Bayankhongor ophiolite mélange, and Osozawa et al. (2008) found similar accreted

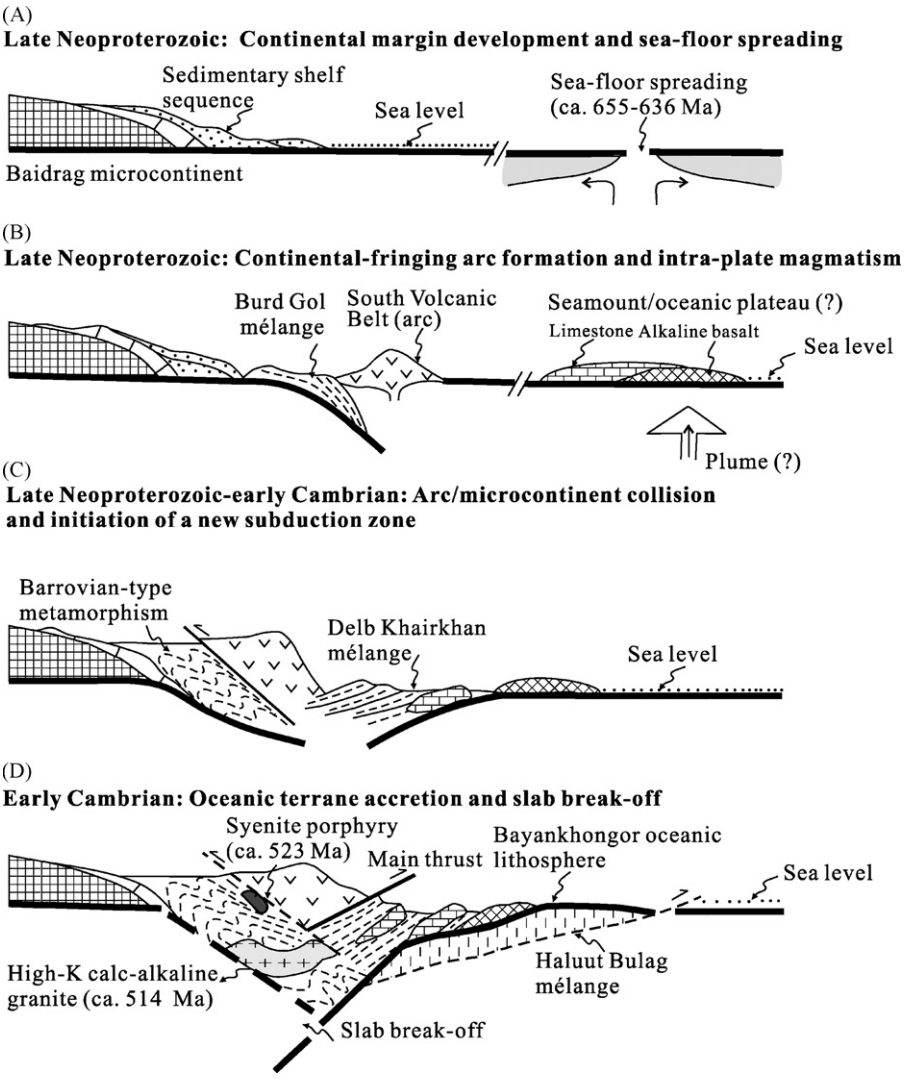

Fig. 9. Interpretive cross-sections of Central Mongolia: (A) On the left (south) is the Baidrag microcontinent with its sedimentary shelf sequence; on the right (north) is an oceanic basin generated by sea-floor spreading. (B) An island arc (South Volcanic Belt) probably formed on an eastward-dipping subduction zone, off the Baidrag microcontinent (left), whereas seamounts or an oceanic plateau (alkaline basalt + limestone ridges) were built on the oceanic crust (right) during drift of the oceanic lithosphere across a hot spot/plume. (C) Arc-microcontinent collision resulted in Barrovian-type metamorphism of the Burd Gol mélange, and a new subduction zone developed along the northern margin of the arc. (D) Due to subduction zone failure/slab break-off, the syenite-porphyry and high-K calc-alkaline granites were emplaced into the convergent continental margin; the Bayankhongor ophiolite was then accreted to the convergent margin by incorporation into and uplift of the two accretionary wedges (the Delb Khairkhan and Haluut Bulag mélanges). Note that the convergent margin (i.e. the arc-microcontinent collision zone) was facing a large oceanic basin, and the ophiolite was emplaced in an intra-oceanic setting.

components throughout the Haluut Bulag mélange. Note that the present data available do not allow a clear distinction between these two settings, i.e., an oceanic plateau or a seamount, which are equally possible.

We therefore propose that the Bayankhongor ophiolite fragments represent an oceanic basement, on which seamount(s) and/or an oceanic plateau formed during the long drift of the oceanic lithosphere.

6.4. Regional evolution in late Neoproterozoic to early Cambrian times

Taking the main south-dipping thrust in Bayankhongor (Fig. 1B) as reference, the hanging wall comprises the South Volcanic Belt (island arc), the Burd Gol accretionary wedge and its Barrovian-type metamorphic belt, the early Paleozoic syenite porphyry and high-K crustal melt granites, and farther south the Baidrag mircocontinent; together these units make up an arc-microcontinent collision zone. The footwall consists of the Delb Khairkhan mélange, the Bayankhongor ophiolite mélange and the Haluut Bulag mélange, which together formed in an oceanic-trench setting.

We now discuss the accretionary and collisional orogeny in central Mongolia. The initial tectonic setting in the Neoproterozoic is likely to have been a wide ocean with drifting microcontinents (e.g. the Baidrag microcontinent), in which sea-floor spreading was active (ca. 655–636 Ma) (Fig. 9A). The arc (South Volcanic Belt) probably formed by subduction of a tract of ocean off the Baidrag microcontinent (Fig. 9B, left). This is based on the argument that the Burd Gol mélange constitutes an accretionary wedge that dips shallowly NE to the south of the South Volcanic Belt (Buchan et al., 2001). Meanwhile, seamounts or an oceanic plateau developed on the ocean crust during drift across a plume/hot spot (Fig. 9B, right). Seamount/oceanic plateau components (limestone and alkali basalt) occur throughout the oceanic terrane (Buchan et al., 2001; Kovach et al., 2005; Tomurtogoo et al., 2006; Osozawa et al., 2008).

Arc-microcontinent collision in the Cambrian resulted in Barrovian–type metamorphism of the Burd Gol mélange (Fig. 9C,

left). Fig. 9C illustrates that, as arc-microcontinent collision was under way, southward subduction began in front of the South Volcanic Belt (arc). Initiation of a subduction zone in response to collision is one of the most important tectonic processes in the modern southwest Pacific (Hall, 2002; Stern, 2004). In central Mongolia, this scenario is supported by the position of the Burd Gol mélange between the South Volcanic Belt and the Baidrag microcontinent (Fig. 1B) and by the fact that the Delb Khairkhan mélange contains material eroded from the South Volcanic Belt (Buchan et al., 2001; Buchan, 2002). At this time the oceanic crust (Bayankhongor ophiolite) was already older than 92 Ma and was locally overlain by seamounts/oceanic plateau. We speculate that arrival of seamounts/oceanic plateau at the trench caused this new south-dipping subduction zone to fail. This process is comparable to the attempted subduction of the Ontong Java Plateau at the Vitiaz Trench (Hall, 2002; Stern, 2004). Oceanic plateaux and large seamounts are generally thought to be buoyant enough to resist subduction (e.g. Cloos, 1993).

After break-off (ca. 523 Ma) of the subducted oceanic slab, the subduction complex began to return to the surface in an intra-oceanic setting (Fig. 9D). The Bayankhongor oceanic lithosphere was thus tectonically dismembered but preserved as a mélange in the turbidite-dominated accretionary wedges (Osozawa et al., 2008). Buchan et al. (2002) suggested that the ophiolite was still undergoing deformation in the early Ordovician (ca. 486 Ma). If correct, uplift may have continued for more than 40 Ma after slab break-off. Deposition and burial of the Dzag sediments (<ca. 446 Ma; see Section 2.1.5) occurred well after tectonic emplacement of the Bayankhongor ophiolite mélange (ca. 523–485 Ma). This invalidates the interpretation of Buchan et al. (2001, 2002) that the Bayankhongor ophiolite was obducted over the Dzag zone that formed part of the passive margin of the Hangai microcontinent.

6.5. Geological significance of the Permo–Triassic mafic rocks

The Permo–Triassic mafic rocks (ca. 298–210 Ma; Table 1) are much younger than the Bayankhongor ophiolite (ca. 655–636 Ma) and have compositions characteristic of magmas produced by partial melting of depleted asthenospheric mantle. However, significant crustal contamination is indicated by the presence of Precambrian zircon xenocrysts ranging in age between 595 and 1825 Ma as well as Paleozoic zircons (see Section 5.2). This implies that continental crust existed beneath the ophiolite mélange prior to magma ascent. In this regard, formation of these mafic rocks was most likely associated with continental rifting, and this explanation is supported by geological evidence that northeast-dipping normal faults occur in the Altan Am area (Fig. 2C) (Natal'in, 2007). These rocks significantly vary in age from one to another and show a relatively large age range (ca. 298–210 Ma), and we attribute them to be the products of episodic rifting. Moreover, the dated Permo-Triassic mafic rocks are all restricted to the ophiolite mélange, and shearing of individual dikes has been observed (Buchan et al., 2001). It is also probable that Permo–Triassic magmatism was accompanied by strike-slip movement along the pre-existing fracture zone of the ophiolite mélange. Natal'in (2007) indicated that strike-slip displacements played a significant role in the formation of the general structural framework of the region. More future work is required to explore the tectonic significance of these newly recognized rocks.

Care must be exercised in investigating ophiolites in which not every "sheeted dike" complex implies an ophiolite; the presence of "sheeted" dikes only indicates an approximate balance between spreading/rifting rate and magma supply (Robinson et al., 2008). On the other hand, the presence of a large and well-developed sheeted dike complex is not a common feature in ophiolites, and the recognition of a sheeted complex should not be a requirement for the definition of this suite of rocks (Robinson et al., 2008).

7. Concluding remarks

Based on our geochemical, Nd–Sr isotopic and zircon age data, the following conclusions are reached: (1) the Bayankhongor oceanic lithosphere originated in a late Neoproterozoic (655 ± 4 Ma to 636 ± 6 Ma), probably wide oceanic basin; (2) the emplacement of a syenite porphyry in the Cambrian (523 ± 2 Ma) reflects the terminal phase of the orogeny; and (3) the ophiolite mélange was affected by Permo-Triassic mafic magmatism which was probably the result of episodic continental rifting, and/or accompanied strike-slip movement.

The Neoproterozoic to Cambrian orogen in central Mongolia evolved in a sequence of events from sea-floor spreading (ca. 655–636 Ma) through intra-oceanic rifting, subduction/arc formation, arc-microcontinent collision (terminated at ca. 523 Ma), and final oceanic terrane accretion. Arc-microcontinent collision may have resulted in initiation of a new subduction zone. As a consequence of jamming of the new subduction zone by seamounts or an oceanic plateau, the old (>92 Ma) Bayankhongor oceanic lithosphere, together with two accretionary wedges, was sutured to a convergent margin facing a large oceanic basin during the terminal phase of orogeny (ca. 523 Ma). Therefore, late Neoproterozoic to Cambrian orogenesis in central Mongolia is comparable, in several aspects, to ongoing orogeny in the southwest Pacific (e.g. Hall, 2002).

Acknowledgements

This paper was significantly improved through comments of B.M. Jahn and B. Natal'in as well as editorial comments of P.A. Cawood. The National Natural Science Foundation of China (grants Nos. 40234045 and 40672048) supported this research.

Appendix A. Supplementary data

Supplementary data associated with this article can be found, in the online version, at doi:10.1016/j.precamres.2009.11.009.

References

Abbotts, I.L., 1981. Masirah (Oman) ophiolite sheeted dikes and pillow lavas: geochemical evidence of the former ocean ridge environment. Lithos 14, 283–294.
Anonymous, 1972. Penrose field conference on ophiolites. Geotimes 17, 24–25.
Arenas, R., Martínez Catalán, J.R., 2003. Low-P metamorphism following a Barrovian-type evolution. Complex tectonic controls for a common transition, as deduced in the Mondonedo thrust sheet (NW Iberian Massif). Tectonophysics 365, 143–164.
Atherton, M.P., Ghani, A.A., 2002. Slab breakoff: a model for Caledonian, Late Granite syn-collisional magmatism in the orthotectonic (metamorphic) zone of Scotland and Donegal, Ireland. Lithos 62, 65–85.
Badarch, G., Cunningham, W.D., Windley, B.F., 2002. A new terrane subdivision for Mongolia: implications for the Phanerozoic crustal growth of Central Asia. Journal of Asian Earth Sciences 21, 87–104.
Bailey, J.C., 1981. Geochemical criteria for a refined tectonic discrimination of orogenic andesites. Chemical Geology 32, 139–154.
Black, L.P., Jagodzinski, E.A., 2003. Importance of establishing sources of uncertainty for the derivation of reliable SHRIMP ages. Australian Journal of Earth Sciences 50, 503–512.
Boudier, F., Nicolas, A., Ildefonse, B., 1996. Magma chambers in the Oman ophiolite: fed from the top and the bottom. Earth and Planetary Science Letters 144, 239–250.
Buchan, C., Cunningham, D., Windley, B.F., Tomurhuu, D., 2001. Structure and lithological charecteristics of the Bayankhongor ophiolite zone, Central Mongolia. Journal of the Geological Society, London 158, 445–460.
Buchan, C., Pfänder, J., Kröner, A., Brewer, T.S., Tomurtogoo, O., Tomurhuu, D., Cunningham, D., Windley, B.F., 2002. Timing of accretion and collisional deformation in the Central Asian Orogenic Belt: implications of granite geochronology in the Bayankhongor Ophiolite Zone. Chemical Geology 192, 23–45.
Buchan, C., 2002. Tectonic evolution of the Bayankhongor ophiolite, Central Mongolia: implications for the Palaeozoic crustal growth of Central Asia. PhD Thesis, University of Leicester, Leicester, 179 pp.
Coleman, R.G., Peterman, Z.E., 1975. Oceanic plagiogranite. Journal of Geophysical Research 80, 1099–1108.

Coleman, R.G., 1977. Ophiolites: Ancient Oceanic Lithosphere. Spinger-Verlag, New York, pp. 1–229.
Coleman, R.G., 1989. Continental growth of northwest China. Tectonics 8, 621–635.
Compston, W., Williams, I.S., Kirschvink, J.L., Zhang, Z., Ma, G., 1992. Zircon U–Pb ages for the Early Cambrian time-scale. Journal of the Geological Society, London 149, 171–184.
Coogan, L.A., Thompson, G., MacLeod, C.J., 2002. A textural and geochemical investigation of high level gabbros from the Oman ophiolite: implications for the role of the axial magma chamber at fast-spreading ridges. Lithos 63, 67–82.
Cloos, M., 1993. Lithospheric buoyancy and collisional orogenesis: subduction of oceanic plateaus, continental margins, island arcs, spreading ridges, and seamounts. Geological Society of America Bulletin 105, 715–737.
Corfu, F., Hanchar, J.M., Hoskin, P.W.O., Kinny, P., 2003. Atlas of zircon textures. In: Hanchar, J.M., Hoskin, P.W.O. (Eds.), Zircon, vol. 53. Reviews in Mineralogy and Geochemistry, pp. 469–500.
Cumming, G.L., Richards, J.R., 1975. Ore lead isotope ratios in a continuously changing earth. Earth and Planetary Science Letters 28, 155–171.
Davies, J.H., von Blanckenburg, F., 1995. Slab breakoff: a model of lithosphere detachment and its test in the magmatism and deformation of collisional orogens. Earth and Planetary Science Letters 129, 85–102.
Demoux, D., Kröner, A., Badarch, G., Jian, P., Tomurhuu, D., Michael, T.D.W., 2009. Geochronological constraints on Cambrian accretion-related magmatism in central Mongolia: evidence from the Bayankhongor and Baydrag terrains. Journal of Geology 117, 377–397.
Dilek, Y., Harald, F., Skjerlie, K.P., 1997. Propagating rift tectonics of a Caledonian marginal basin: multi-stage seafloor spreading history of the Solund-Stavfjord ophiolite in western Norway. Tectonophysics 280, 213–238.
Dilek, Y., 2003. Ophiolite concept and its evolution. In: Dilek, Y., Newcombe, S. (Eds.), Ophiolite Concept and the Evolution of Geological Thought, vol. 373. Geological Society of America (Special Paper), pp. 1–16.
Dubińskaa, E., Bylinab, P., Kozlowskia, A., Dörrc, W., Nejbertd, K., Schastokc, J., Kulickie, C., 2004. U–Pb dating of serpentinization: hydrothermal zircon from a metasomatic rodingite shell (Sudetic ophiolite, SW Poland). Chemical Geology 203, 183–203.
Gill, R.C.O., Aparicio, A., Azzouzi, M.E., Hernandez, J., Thirlwall, M.F., Bourgois, J., Marriner, G.F., 2004. Depleted arc volcanism in the Alboran Sea and shoshonitic volcanism in Morocco: geochemical and isotopic constraints on Neogene tectonic processes. Lithos 78, 363–388.
Hall, R., 2002. Cenozoic geological and plate tectonic evolution of SE Asia and the SW Pacific: computer-based reconstructions, model and animations. Journal of Asian Earth Sciences 20, 353–431.
Hofmann, A.W., 1988. Chemical differentiation of the Earth: the relationship between mantle, continental crust, and oceanic crust. Earth and Planetary Science Letters 90, 297–314.
Hopson, C.A., Mattinson, J.M., Pessagno Jr., E.A., Luyendyk, B.P., 2008. California Coast Range ophiolite: composite middle and late Jurassic oceanic lithosphere. Geological Society of America Special paper 438, 1–101, doi: 10.1130/2008.2438(01).
Isozaki, Y., Maruyama, S., Furuoka, F., 1990. Accreted oceanic materials in Japan. Tectonophysics 181, 179–205.
Jahn, B.M., Wu, F.Y., Chen, B., 2000. Granitoids of the Central Asian Orogenic Belt and continental growth in the Phanerozoic. Transactions of Royal Society, Edinburgh, Earth Sciences 91, 181–193.
Jahn, B.M., Capdevila, R., Liu, D.Y., Vernon, A., Badarch, G., 2004. Sources of Phanerozoic granitoids in the transect Bayankhongor-Ulaan Baatar, Mongolia: geochemical and Nd isotopic evidence, and implications for Phanerozoic crustal growth. Journal of Asian Earth Sciences 23, 629–653.
Jahn, B.M., Litvinovsky, B.A., Zanvilevich, A.N., Reichow, M., 2009. Peralkaline granitoid magmatism in the Mongolian–Transbaikalian Belt: Evolution, petrogenesis and tectonic significance. Lithos, doi:10.1016/j.lithos.2009.06.015.
Kelemen, P.B., Aharonov, E., 1998. Periodic formation of magma fractures and generation of layered gabbros in the lower crust beneath oceanic spreading ridges. In: Buck, W.R. (Ed.), Faulting and Magmatism at Mid-Ocean Ridges, Geophysical Monograph Series, vol. 106. AGU, Washington, DC, pp. 267–289.
Kepezhinskas, P.K., Kepezhinskas, K.B., Pukhtel, I.S., 1991. Lower Paleozoic oceanic crust in Mongolian Caledonides: Sm–Nd isotope and trace element data. Geophysical Research Letters 18, 1301–1304.
Kerr, A.C., Tarney, J., Nivia, A., Marriner, G.F., Saunders, A.D., 1998. The internal structure of oceanic plateaus: inferences from obducted Cretaceous terranes in western Colombia and the Caribbean. Tectonophysics 292, 173–188.
Khain, E.V., Bibikova, E.V., Kröner, A., Zhuravlev, D.Z., Sklyarov, E.V., Fedotova, A.A., Kravchenko-Berezhnoy, I.R., 2002. The most ancient ophiolite of the Central Asian fold belt: U–Pb and Pb–Pb zircon ages for the Dunzhugur Complex, Eastern Sayan, Siberia, and geodynamic implications. Earth and Planetary Science Letters 199, 311–325.
Khain, E.V., Bibikova, E.V., Salnikova, E.B., Kröner, A., Gibsher, A.S., Didenko, A.N., Degtyarev, K.E., Fedotova, A.A., 2003. The Palaeo-Asian ocean in the Neoproterozoic and early Paleozoic: new geochronologic data and palaeotectonic reconstructions. Precambrian Research 122, 329–358.
Kimura, G., Ludden, J., 1995. Peeling oceanic crust in subduction zones. Geology 23, 217–220.
Kotov, A.B., Kozakov, I.K., Bibikova, E.V., 1995. Duration of regional metamorphic episodes in areas of polycyclic endogenic processes: a U–Pb geochronological study. Journal of Petrology 3, 567–575.
Kovach, V.P., Jian, P., Yarmolyuk, V.V., Kozakov, I.K., Liu, D.Y., Terenteva, L.B., Lebedev, V.I., Kovalenko, R.V.I., 2005. Magmatism and geodynamics of early stages of the Paleoasian Ocean formation: geochronological and geochemical data on ophiolites of the Bayan-Khongor zone. Doklady Earth Science 104, 1072–1077.
Kozakov, I.K., Kotov, A.B., Salnikova, E.B., Kovach, V.P., Nutman, A.P., Bibikova, T.I., Kirnozova, T.I., Todt, W., Kröner, A., Yakovleva, S.Z., Lebedev, V.I., Sugorakova, A.M., 2001. Timing of the structure evolution of metamorphic rocks in the Tuva-Mongolian Massif. Geotectonics 35, 165–184.
Kozakov, I.K., Sal'nikova, E.B., Yakovleva, S.Z., Plotkina, Y.V., Fedoseenko, A.M., 2006. Vendian metamorphism in the accretionary-collisional structure of central Asia. Doklady Earth Science 407, 192–197.
Kröner, A., Windley, B.F., Badarch, G., 2007. Accretionary growth and crust-formation in the Central Asian Orogenic Belt and comparison with the Arabian-Nubian shield. Geological Society America Memoir 200, 181–209.
Kovalenko, V.I., Yarmolyuk, V.V., Kovach, V.P., Kotov, A.B., Kozlovsky, A.M., Salnikova, E.B., Larin, A.M., 2004. Isotope provinces, mechanisms of generation and sources of the continental crust in the Central Asian Mobile Belt: geological and isotopic evidence. Journal of Asian Earth Sciences 23, 605–627.
Kuzmichev, A., Kröner, A., Hegner, E., Liu, D., Wan, Y., 2005. The Shishkid ophiolite, northern Mongolia: a key to the reconstruction of a Neoproterozoic island arc system in central Asia. Precambrian Research 138, 125–150.
Kurimoto, C., Tungalag, F., 1998. K–Ar ages of white micas from politic schists of the Bayankhongor area, west Mongolia. Bulletin of Geological Survey of Japan 49, 19–23.
Le Bas, M., Le Maitre, R.W., Streckeisen, A., Zanetin, A., 1986. A chemical classification of volcanic rocks based on the total alkali-silica diagram. Journal of Petrology 27, 745–750.
Le Maitre, R.W., Bateman, P., Dudek, A., Keller, J., Le Bas, M., Sabine, P.A., Schmid, R., Sorensen, H., Streckeisen, A., Woolley, A.R., Zanettin, B., 1989. A Classification of Igneous Rocks and a Glossary of Terms. Recommendations of the IGUS Sub-commission on the Systematic of Igneous Rocks. Blackwell, Oxford.
Lissenberg, C.J., Bédard, J.H., van Staal, C.R., 2004. The structure and geochemistry of the gabbro zone of the Annieopsquotch ophiolite, Newfoundland: implications for lower crustal accretion at spreading ridges. Earth and Planetary Science Letters 229, 105–123.
Macdonald, R., Hawkesworth, C.J., Heath, E., 2000. The Lesser Antilles volcanic chain: a study in arc magmatism. Earth-Science Review 49, 1–76.
Malpas, J., Sporli, K.B., Black, P.M., Philippa, M., Smith, I.E.M., 1992. Northland ophiolite, New Zealand, and implication for plate-tectonic evolution of the southwest Pacific. Geology 20, 149–152.
Maruyama, S., 1997. Pacific-type orogeny revisited: Miyashiro-type orogeny proposed. The Island Arc 6, 91–120.
Masuda, A., Nakamura, N., Tanaka, T., 1973. Fine structures of mutually normalized rare-earth patterns of chondrites. Geochimica et Cosmochimica Acta 37, 239–248.
Mitrofanov, F.P., Kozakov, I.K., Palay, I.P., 1981. Precambrian of western Mongolia and southern Tuva. In: Transactions of the Joint Soviet-Mongolian Scientific Research Geological Expedition, vol. 32. Nauka, Leningrad, p. 156 (in Russian).
Menzies, M.A., Kyle, P.R., Jones, P.R., Ingram, G., 1991. Enriched and depleted source components for tholeiitic and alkaline lavas from Zuni-Bandera, New Mexico: inferences about intraplate processes and stratified lithosphere. Journal of Geophysical Research 96, 13645–13671.
Meyer, J., Mercolli, I., Immenhauser, A., 1996. Off-ridge alkaline magmatism and seamount volcanoes in the Masirah island ophiolite, Oman. Tectonophysics 267, 187–208.
Moores, E.M., 1982. Origin and emplacement of ophiolites. Reviews of Geophysics and Space Physics 20, 735–760.
Morrison, G.W., 1980. Characteristics and tectonic setting of the shoshonite rock association. Lithos 13, 97–109.
McCulloch, M.T., Perfit, M.R., 1981. $^{143}Nd/^{144}Nd$, $^{87}Sr/^{86}Sr$ and trace element constraints on the petrogenesis of Aleutian island arc magmas. Earth and Planetary Science Letters 56, 167–179.
McCulloch, M.T., Cameron, W.E., 1983. Nd–Sr isotopic study of primitive lavas from the Troodos ophiolite, Cyprus: evidence for a subduction-related setting. Geology 11, 727–731.
Natal'in, B., 2007. Tectonics of Mongolia: the second workshop of the IGCP-480 project "Tectonics of Central Asia". Episodes, March 1–7.
Nelson, B.K., DePaolo, D.J., 1984. Rapid production of continental crust 1.7 to 1.9 b.y. ago: Nd isotopic evidence from the basement of the North American midcontinent. Geological Society of America Bulletin 96, 746–754.
Nicolas, A., 1989. Structures of Ophiolites and Dynamics of Oceanic Lithosphere. Kluwer Academic Publisher, Dororecht/Boston/London, pp. 1–369.
Osozawa, S., Tsolmon, G., Majigsuren, U., Sereenen, J., Niisuma, S., Iwata, W., Pavils, T., Jahn, B.M., 2008. Structural evolution of the Bayankhongor region, west-central Mongolia. Journal of Asian Earth Sciences 33, 337–352.
Pamic, J., Balen, D., Herak, M., 2002. Origin and geodynamic evolution of Late Paleogene magmatic associations along the Periadriatic-Sava-Vardar magmatic belt. Geodinamica Acta 15, 209–231.
Pearce, J.A., Harris, S.W., Tindle, A.G., 1984. Trace element discrimination diagrams for the tectonic interpretation of granitic rocks. Journal of Petrology 25, 956–983.
Peters, T.J., Menzies, M.A., Thirlwall, M.F., Kyle, P.R., 2008. Zuni-Bandera volcanism, Rio Grande, USA—melt formation in garnet- and spinel-facies mantle straddling the asthenosphere-lithosphere boundary. Lithos 102, 295–315.
Rippington, S., Cummingham, D., England, R., 2008. Structure and petrology of the Altan Uul Ophiolite: new evidence for a Late Carboniferous suture in the Gobi Altai, southern Mongolia. Journal of the Geological Society, London (165), 711–723.

Robinson, R.T., Malpas, J., Dilek, Y., Zhou, M.F., 2008. The significance of sheeted dike complexes in ophiolites. GSA Today 18 (no. 11), doi:10.1130/GSATG22A.1.

Sengör, A.M.C., Natal'in, B.A., Burtman, V.S., 1993. Evolution of the Altaid tectonic collage and Paleozoic crustal growth in Eurasia. Nature 364, 299–307.

Sengör, A.M.C., Natal'in, B.A., 1996. Turkic-type orogeny and its role in the making of the continental crust. Annual Review of Earth and Planetary Sciences 24, 263–337.

Sengör, A.M.C., Natal'in, B.A., 2004. Phanerozoic analogues of Archaean oceanic basement fragments: Altaid ophiolites and ophirags. In: Kusky, T.M. (Ed.), Precambrian Ophiolites and Related Rocks. Elsevier, Amsterdam, pp. 675–726.

Spaggiari, C.V., Gray, D.R., Foster, D.A., 2004. Ophiolite accretion in the Lachlan Orogen, Southeastern Australia. Journal of Structural Geology 26, 87–112.

Stern, R.J., 2004. Subduction initiation: spontaneous and induced. Earth and Planetary Science Letters 226, 275–292.

Steiger, R.H., Jäger, E., 1977. Subcommission on geochronology: Convention on the use of decay constants in geo- and cosmochronology. Earth and Planetary Science Letters 36, 359–362.

Teraoka, Y., Suzuki, M., Tungalag, F., Ichinnorov, N., Sakamaki, Y., 1996. Tectonic framework of the Bayankhongor area, west Mongolia. Bulletin of the Geological Survey of Japan 47, 447–455.

Thompson, A.B., England, P.C., 1984. Pressure-temperature-time paths of regional metamorphism: II. Their inference and interpretation using mineral assemblages in metamorphic rocks. Journal of Petrology 25, 929–955.

Tomurtogoo, O., Tomurkhuu, D., Erdenesaikhan, G., Kröner, A., Demoux, A., Rojas-Agramonte, Y., 2006. Excursion in Central and Southern Mongolia. Structure and Tectonic Correlation Across the Central Orogenic Collage: Implications for Continental Growth and Intracontinental Deformation. Abstracts and Excursion Guidebook, IGCP480. Institute of Geology and Mineral Resources, Mongolian Academy of Science, Ulaanbaatar, Mongolia, pp. 107–146.

Turner, S., Arnaud, N., Liu, J., Rogers, N., Hawkesworth, C., Harris, N., Kelley, S., van Calstern, P., Deng, W., 1996. Post-collision, shoshonitic volcanism on the Tibetan Plateau: implications for convective thinning of the lithosphere and the source of ocean island basalts. Journal of Petrology 37, 45–71.

Wakabayashi, J., Dilek, Y., 2003. What constitutes 'emplacement' of an ophiolite?: mechanisms and relationship to subduction initiation and formation of metamorphic soles. In: Dilek, Y., Robinson, P.T. (Eds.), Ophiolites in Earth History, 218. Special Publications, Geological Society, London, pp. 427–447.

Whalen, J.B., McNicoll, V.J., van Staak, C.R., Lissenberg, C.J., Longstaffe, F.J., Jenner, G.A., van Breeman, O., 2006. Spatial, temporal and geochemical characteristics of Silurian collision-zone magmatism, Newfoundland Appalachians: An example of a rapidly evolving magmatic system related to slab break-off. Lithos 89, 377–404.

Williams, I.S., Buick, I.S., Cartwright, I., 1996. An extended episode of early Mesoproterozoic metamorphic fluid flow in the Reynolds Range, central Australia. Journal of Metamorphic Geology 14, 29–47.

Windley, B.F., Alexeiev, D., Xiao, W.J., Kröner, A., Badarch, G., 2007. Tectonic models for accretion of the Central Asian Orogenic Belt. Journal of the Geological Society, London 164, 31–47.